Kufa Journal of Engineering
Vol. 17, No. 2, April 2026, P.P. 542-576
Article history: Received 3 May 2025, last revised 14 August 2025, accepted 16 August 2025

STABILITY SOLUTION FOR THE 220 KV POWER GRID INTEGRATED WITH RENEWABLE ENERGY SOURCE USING BESS: A CASE STUDY OF VIETNAM

Dinh Nho Thu[1], Le Van Dai[1,*], Le Cao Quyen[1], Tran Viet Thanh[2], and Pham Hong Thanh[3]

[1] Faculty of Electrical Engineering Technology, Industrial University of Ho Chi Minh City, Ho Chi Minh City, Vietnam.

[2] Power Engineering Consulting Joint Stock Company 4, Nha Trang, Khanh Hoa, Vietnam.

[3] Thu Dau Mot University, Vietnam.

***Corresponding author email: levandai@iuh.edu.vn**

https://doi.org/10.30572/2018/KJE/170233

ABSTRACT

This paper proposes a control method for battery energy storage systems (BESS) connected to a 220 kV transmission network to enhance grid stability when renewable energy sources (RES), such as wind and solar, are integrated. This problem leads to significant issues developing for grid stability, including frequency instability, transmission line overloads, and grid failures. The research mainly focuses on the 220 kV transmission line between the 500 kV Pleiku and Dak Nong substations in Vietnam's Tay Nguyen area. Using PSS®E and DigSILENT Power Factory modeling tools, the findings reveal that combining three BESS units, each with a rated power capacity of 200 MW and an energy storage capacity of 673 MWh, effectively reduces grid congestion and stabilizes frequency fluctuations. Simulation findings estimate a decrease of 2,057 MWh in surplus power production. in case with the BESS connection, the minimum system frequency during rapid RES production increases to 49.17 Hz, up from 48.91 Hz without BESS, ensuring that power flows remain within acceptable operating limits. These simulation results illustrate the proposed method BESS, can enhance grid performance, decrease faults, preserve frequency stability during RES fluctuation, and facilitate Vietnam's clean energy transition, notably in the Tay Nguyen area. This proposed method also meets the frequency stability standards outlined in Circular No. 25/2016/TT-BCT issued by the Vietnamese Ministry of Industry and Trade.

KEYWORDS

Battery energy storage systems (BESS); transmission corridor analysis; frequency response; renewable power variability; power system operation.

1. INTRODUCTION

Power systems worldwide are experiencing rapid increases in wind and solar generation, driven by long-term decarbonization targets rather than by short-term policy adjustments alone. The commitments announced at the COP28 conference in December 2023, which aim to triple global renewable energy capacity to at least 11,000 GW by 2030 in support of the Paris Agreement's 1.5 °C objective, are expected to accelerate this trend further. Consequently, variable renewable energy (VRE), dominated by wind and solar power, is projected to account for approximately two-thirds of global renewable electricity generation by 2030, compared with less than 45% at present. This expansion is primarily attributed to the rapid scale-up of solar capacity and the continued growth of onshore and offshore wind generation.

In Vietnam, the large-scale integration of wind and solar power has revealed practical challenges in grid integration and regulatory coordination, temporarily constraining project development. However, as market mechanisms and transmission infrastructure evolve, these limits are projected to be gradually abolished by 2030. With this trend, Vietnam is well-positioned to meet its renewable energy goals and continue to play a prominent role in the ASEAN region, accounting for approximately 40% of the expansion in renewable capacity. As a result, wind and solar photovoltaic generation are increasingly becoming dominant contributors to the national electricity supply, as illustrated in Fig. 1.

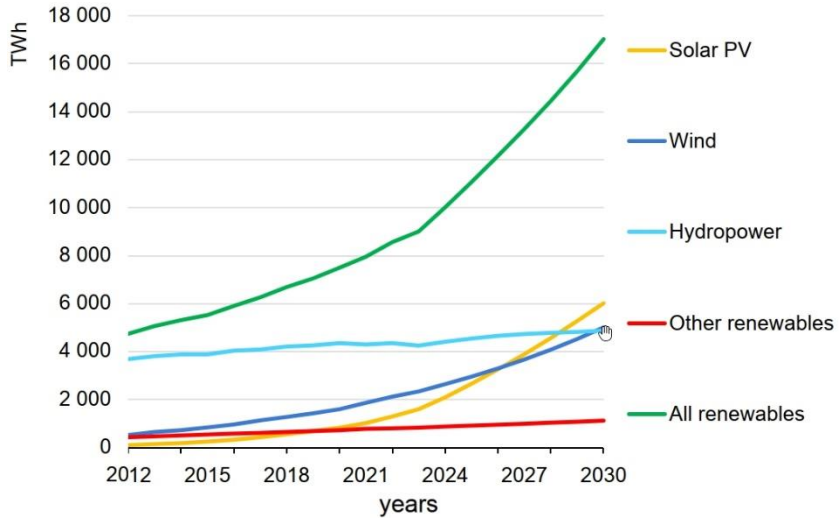

Fig. 1. Technological evolution in global electricity generation, 2000-2030

As wind and solar photovoltaic energy progressively contribute to the electricity supply, new operational issues develop for power system stability. Although renewable energy deployment delivers substantial environmental benefits, wind and solar resources are inherently variable and are typically connected to the grid via power electronic interfaces, leading to non-synchronous operation. This property minimizes effective system inertia. In traditional power

systems, inertia is generally provided by synchronous generators and plays a crucial role in controlling the pace and magnitude of frequency variations following unexpected power imbalances. As the penetration of renewable energy sources (RES) increases, the loss of system inertia makes the grid more prone to frequency excursions and oscillatory behavior. For the case of severe disruptions, these effects may trigger under-frequency load shedding (UFLS) systems, thereby posing a threat to overall system dependability.

The reduction of system inertia has shifted from a theoretical concern to a practical operating issue in power systems with high renewable penetration. In this context, BESSs are not introduced as general supporting technologies, but rather as controllable resources capable of responding rapidly to power imbalances. From a system operations perspective, BESSs can inject or absorb active power quickly, making them suitable for supporting frequency dynamics and facilitating the integration of renewable energy.

The use of battery energy storage systems (BESS) has developed rapidly. According to data from the International Renewable Energy Agency, BESS installations globally increased from around 0.1 GWh in 2010 to over 95.9 GWh in 2023, as shown in Fig. 2. Newly installed capacity was over three times more than that of the previous year, most significantly in China and the US. Furthermore, the cost of installing this equipment also decreased significantly; the average project cost dropped from almost 2,700 USD/kWh in 2010 to 273 USD/kWh in 2023, indicating that the cost barrier for installation is not a major issue for large projects.

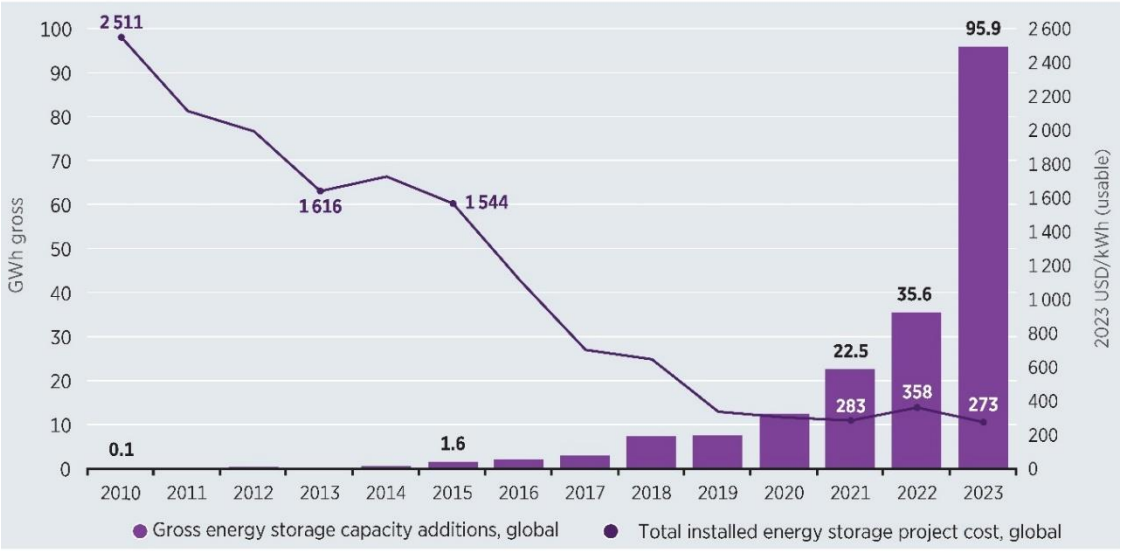

Fig. 2. Year-by-year battery energy storage capacity additions and associated project cost levels

Vietnam's power system is structured across multiple voltage levels. The 500 kV transmission line acts as the main circuit, connecting power sources and loads between the North, Central, and South regions. Currently, renewable energy development is largely concentrated in the

South Central Coast and Tay Nguyen areas, where a growing number of wind and solar plants are being commissioned. Once renewable energy sources supply sufficient capacity, the regional power system faces overload. The impact is most evident in Tay Nguyen, where a significant share of renewable generation is connected directly to the 220 kV and 110 kV grids rather than to the 500 kV backbone. Currently, this system is overloaded and requires attention and concern from the transmission sector.

According to Decision No. 500/QD-TTg issued by the Prime Minister of Vietnam in 2023 (Vietnam-Prime-Minister, 2023), through the National Power Development Plan (PDP8), energy storage has been explicitly defined as a solution for large-scale renewable energy integration. Following this direction, the total installed storage capacity is projected to reach roughly 2,700 MW by 2030, including around 2,400 MW of pumped-storage hydropower and 300 MW of pumped-storage energy systems (BESS). The planned deployment of BESS rises dramatically from 2030 onwards, with total storage capacity predicted to reach the range of 30,650 - 45,550 MW by 2050. Thus, BESS is considered an operational solution to help stabilize grid-connected renewable energy sources. Under this policy, BESS is considered operational equipment, not equipment used for capacity expansion

Integrating BESS into the national grid is not a straightforward task and introduces several practical technical challenges. From an operational perspective, these challenges are mainly associated with control strategy design and site selection. To operate effectively with intermittent wind and solar generation, BESS must be equipped with control schemes that respond to rapid power fluctuations rather than relying solely on forecast-based scheduling. In addition, grid-connected BESS requires coordinated synchronization with nearby renewable plants to ensure stable and efficient operation under changing system conditions. The deployment of BESS is also dependent on different factors, such as limited land availability and non-uniform grid connectivity, which are particularly evident in rural and weakly interconnected areas.

BESS has been investigated and deployed in power systems for several decades, initially for load balancing and ancillary services. When the penetration of intermittent renewable energy sources (RES) has increased, the role of BESS has gradually shifted toward supporting system operation under variable generation conditions. In modern power systems, BESS is commonly applied to enhance operational flexibility and to mitigate the variability associated with wind and photovoltaic (PV) generation. Owing to their complementary production profiles, the joint integration of wind and solar PV has attracted increasing attention in recent years. Recent figures suggest that grid-scale installations integrating both RES resources have reached around

41.84 GWh of power capacity and 104.67 GWh of energy capacity globally, which demonstrates the increased dependence on storage-supported renewable generation (Frost & Sullivan, 2024).

Legacy generating fleets offer a natural buffer via mechanical inertia, a trait lost in grids with RES. To ensure frequency stability, the system increasingly depends on the speed and agility of contemporary balancing assets. This is where BESS becomes essential. By capturing excess energy during peak renewable windows and filling the gaps during low res intervals, these systems act as the grid's primary stabilizer (Chen et al., 2015). To sharpen the system's dynamic response, researchers have explored various methodologies, most notably virtual inertia emulation, droop-based logic, and synergistic operation with res (Li et al., 2023). However, the operational impact of BESS is inseparable from its physical scale and site selection, both of which govern the trade-off between technical gains and financial outlay. To address this, numerous optimisation algorithms and planning strategies have been formulated to tailor BESS deployment to specific grid requirements (Alsharif et al., 2022; Khunkitti et al., 2022).

BESS efficiency depends on the capacity, placement, and control method together with state of charge (*SoC*) management (Sadeq Al Khudairi & Vural, 2024). Because of this, many optimization methods now exist in literature. Such as, some studies use math models to find the best BESS locations for frequency stability (Lee et al., 2023). Others prefer swarm-based tools. In particular, particle swarm optimization (PSO) helps tune parameters to stop frequency swings during res surges or grid faults (Nguyen et al., 2024). Similarly, the grey wolf optimizer is used to size systems to handle big gaps between generation and load (El-Bidairi et al., 2020). But these methods have a real problem. They take too much computing power. This makes it hard to use them in large, real-world power grids where speed is everything.

Beyond frequency-oriented optimization, multi-objective assessment frameworks have been introduced to maximize BESS capacity while accounting for technical and economic (Teh & Lai, 2019). Other studies have focused on improving operational efficiency and economic performance at the distribution level, for example, by implementing BESS models in OpenDSS environments (Maeyaert et al., 2020). However, such approaches frequently rely on simplified economic assumptions or lack compatibility with broader market-based simulation tools, thereby restricting their applicability in realistic grid scenarios. Alternative swarm intelligence techniques, such as the artificial bee colony optimization, have been explored to reduce frequency deviations and size optimize (Das et al., 2020). Despite their effectiveness, these methods are prone to local optima and are highly sensitive to tuning the parameter. More recent placement and sizing strategies have attempted to link BESS deployment with system demand

and generation profiles (Alsharif et al., 2022). Nevertheless, assumptions such as constant battery internal resistance and fixed BESS parameters overlook practical variations caused by temperature and *SoC* dynamics, and their validation has often been limited to benchmark systems such as the IEEE 39-bus network.

After analyzing the studies above, it can be concluded that BESS connected to the electrical system with multiple integrated PV sources can continuously control power, ensure stable electricity generation, or perform load shifting, adjusting the electricity output according to peak demand and reducing peak load pressure. This study provides the usage of BESS to relieve surplus power from the energy source by estimating capacity, location, and control method.

The main contribution of this research is focusing on controlling the BESS device to stabilize the 220 kV power grid when multiple renewable energy sources are integrated, with the aim of minimizing overload and stabilizing voltage. The major purpose of the research is to maximize the use of BESS to protect the stability of the grid during rapid swings in power output from renewable sources. To achieve this purpose, the following goals are addressed:

i) Analysis of the power flow over time to estimate the influence of renewable energy sources on Vietnam's 220 kV transmission system;

ii) Development of the technology to detect location, compute capacity, and optimize control of the BESS;

iii) Evaluation and analysis of the operational capabilities of the transmission line after connecting the BESS in diverse scenarios, such as power flow, the frequency effect when the energy source unexpectedly falls in power production, and grid failures.

This paper is organized as follows: Section 2 describes the studied power system and outlines the main operational challenges arising from renewable energy integration, with a focus on the 220 kV transmission network in Vietnam. Section 3 analyzes congestion issues in the 220 kV grid caused by increasing wind and solar power output, particularly along heavily loaded transmission corridors. Section 4 presents the method for determining capacity and designing the control strategy of BESS. Section 5 analyses the simulation results and evaluates system performance under other operating conditions. Finally, Section 6 summarizes the study's main conclusions.

2. THE STUDIED TRANSMISSION NETWORK

2.1. Transmission network mode

Dak Lak is a province in the Tay Nguyen region of Vietnam, endowed with significant potential

for developing medium and small-scale hydropower resources. The province's electricity supply is primarily derived from medium and small-sized hydropower plants (HPs) within the region. As of now, the total installed capacity of the 13 operational HPs in Dak Lak is 79.52 MW. Additionally, six large-scale hydropower plants with a combined capacity of 794 MW, five solar power plants with a total capacity of 991.65 MWp, and rooftop solar systems with a total capacity of 373.59 MWp connected to the medium and low-voltage grids, contribute significantly to the electricity supply for the Tay Nguyen region and the national power grid.

The 220 kV transmission system, represented in the single-line scheme in Fig. 3, connects the 500/220 kV Pleiku with Dak Nong substation. This strategy has been devised to manage challenges such as overloads. It includes of 735.03 kilometers of 220 kV transmission lines and 94.4 kilometers of 500 kV transmission lines. The system has four hydropower plants (HPs) with a total capacity of 450 MW, namely Tua Srah (86 MW), Serepok 3 (220 MW), Serepok 4A (64 MW), and Serepok 4 (80 MW). It also includes six photovoltaic (PV) farms with a total capacity of 1,280 MWp, namely Xuan Thien Ea Sup (820 MWp), Cu Knia (180 MWp), Xuyen Ha (130 MWp), Serepok (50 MWp), Serepok 1 (50 MWp), and Quang Minh (50 MWp), as well as five wind farms (WFs) with a total capacity of 820 MW, including Dak Hoa - Nam Binh 1 (50 MW), Buon Kuop (280 MW), Krong Ana 1 (160 MW), Cu Ne 1, 2 - Krong Buk 1, 2 (100 MW), and Ia Le (100 MW). This system is directly connected to Vietnam's 500/220 kV transmission network.

To develop a calculation model based on the current status and investment plan for power development in line with the objectives outlined above, this report constructs a 110 kV, 220 kV, and 500 kV power grid model for the entire country for the year 2025 using PSS/E software. Subsequently, the power system data will be transferred to DIgSILENT software to create detailed models of solar and wind power plants for the provinces of Binh Thuan, Ninh Thuan, Khanh Hoa, Phu Yen, Binh Dinh, as well as the three provinces in the Tay Nguyen region (Gia Lai, Dak Lak, and Dak Nong), utilizing the static generator model. The quasi-dynamic simulation tool in PowerFactory DIgSILENT software will be employed for 24-hour operational calculations. In addition, the paper focuses on two renewable energy sources that are contributing a large amount of capacity to the grid under consideration, namely PV and WF, which are modeled in Subsection 2.2.

2.2. Renewable Energy Source Models

1) *Photovoltaic plant model*, the PV farms utilize solar panels with the specifications as maximum power output P_{max} (330 W), open-circuit voltage U_{oc} (45.96 V), voltage at maximum

power U_{mpp} (39.11 V), short-circuit current I_{sc} (8.91 A), current at maximum power I_{mpp} (8.45 A), and panel efficiency η (17.1%). The design of the PV arrays is based on the inverter's technical characteristics and the selected system configuration (Al-Jabari et al., 2022). Multiple modules are connected in series to form high-voltage strings that minimize losses. The maximum number of PV panels in a string is determined by the inverter's maximum DC input voltage ($U_{max(inverter,DC)}$). In any configuration, the string's voltage must not exceed the inverter's minimum input voltage. The maximum number of PV panels (n_{max}) in a string is calculated by

$$U_{oc} \cdot n_{max} < U_{max(inverter,DC)}, \quad (1)$$

when the number of PV modules in the string reaches the minimum allowable voltage for system operation, it will be necessary to adjust the number of modules. If the string voltage drops below the inverter's minimum operating voltage, the system will fail to operate or will function inefficiently. Therefore, the minimum number of PV modules (n_{min}) in the string is adjusted to ensure with the following condition

$$U_{mpp} \cdot n_{min} > U_{min(inverter,min)}. \quad (2)$$

The inverter unit is used to convert DC to AC voltage, with a maximum input DC voltage of 1,500 V. The MPPT operating voltage range is 915 - 1300 V, while the output voltage is 630 V, with a rated power of 2550 kW/2550 KVA. The input standard is 16 terminals. The voltage is stepped up from 630 V to 220 kV through a step-up transformer to connect to the 220 kV grid. The connection diagram of the PV farms is shown in Fig. 4.

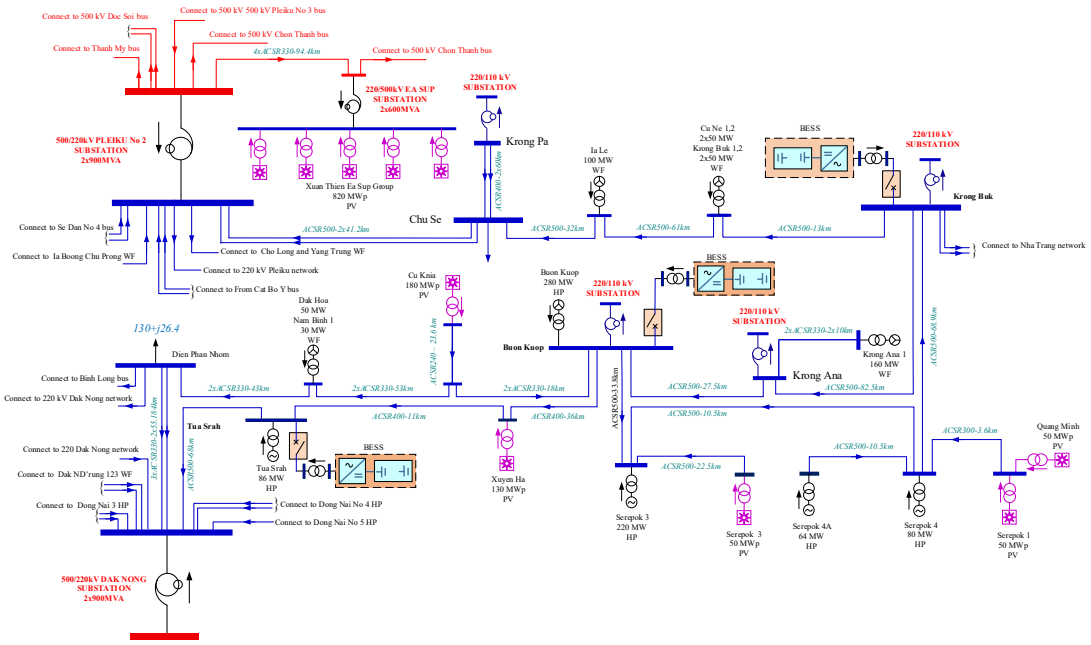

Fig. 3. Single-line diagram of the 500/220 kV transmission corridor linking the Pleiku and Dak Nong substations.

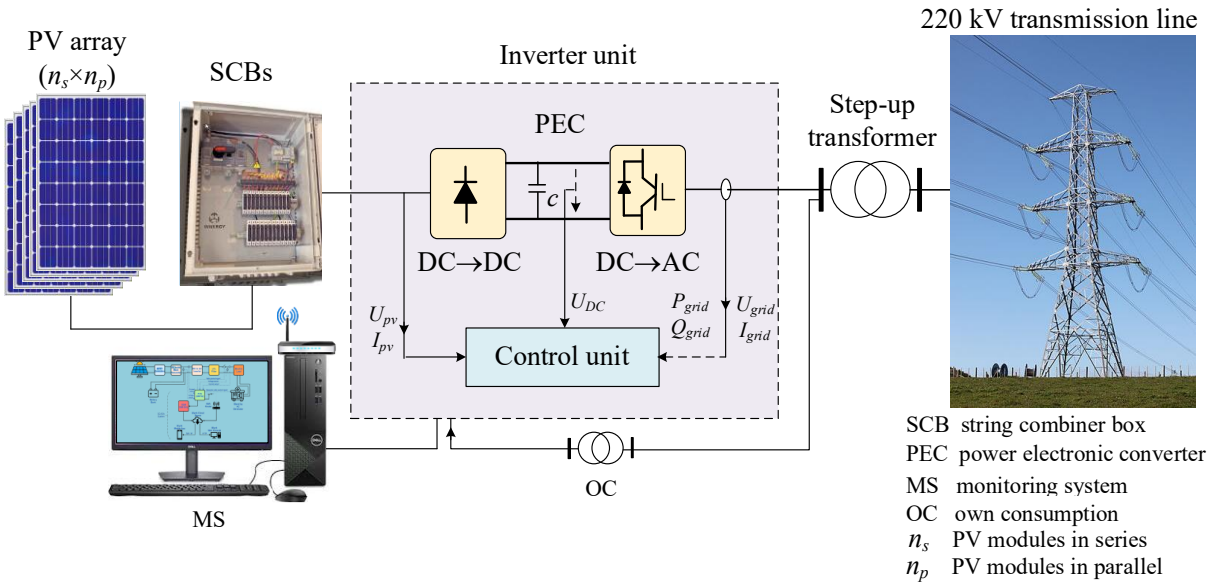

Fig. 4. Overview model of a photovoltaic power plant

The output power of solar PV plants is heavily dependent on solar radiation intensity (G) and ambient temperature (T_M). The relationship between these variables can be expressed using the following equation (Alkahtani et al., 2024; Dhaked et al., 2023; Tripathi et al., 2018)

$$P_{PV} = n \cdot P_{STC} \cdot \frac{G}{G_{STC}} \cdot \left(1 - k \cdot (T_M - T_{STC})\right), \quad (3)$$

where P_{PV} - output power of the PV plant, n - number of PV modules, P_{STC} - maximum power of a module under standard test conditions, G - incident irradiance on the modules (W/m^2), G_{STC} - the irradiance under standard test conditions (1,000W/m^2), k - the power-generation temperature coefficient of PVs (%/ºC), T_M - the temperature of the module (ºC), T_{STC} - the reference temperature (25ºC). The model incorporates hourly solar radiation data derived from meteorological forecasts, as shown in Fig. 5. For instance, during peak solar hours (11:00 - 14:00), the incident irradiance reaches approximately 923.9W/m^2, leading to maximum PV generation.

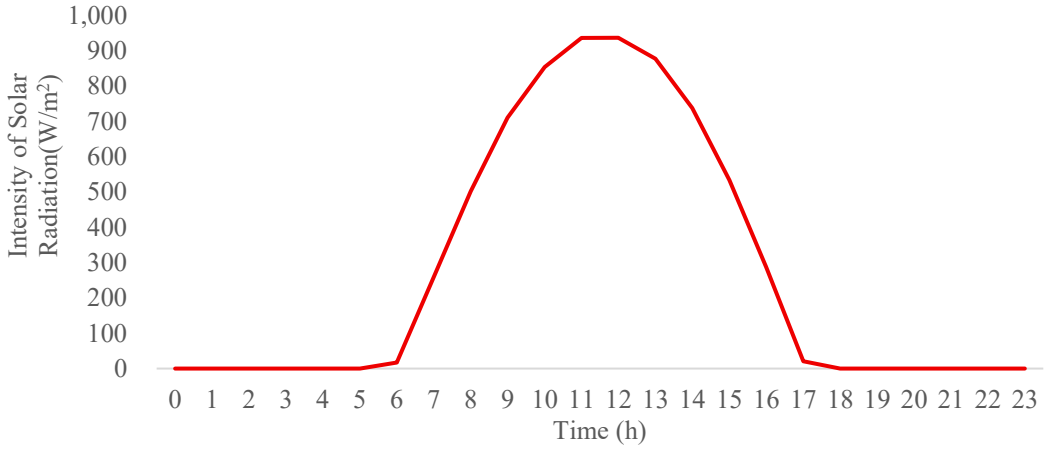

Fig. 5. Solar radiation intensity

2) *Wind farm model*, the wind farm model used in wind power plants is the type 3 wind turbine model. The stator windings are directly connected to the power grid, while the rotor windings are connected to the grid through back-to-back converters, consisting of a rotor-side converter (RSC) and a grid-side converter (GSC), via slip rings. Therefore, the DFIG can both absorb and deliver power from the grid through the rotor windings via the RSC and GSC, while power injection into the grid occurs through the stator windings. The block diagram for the overall control strategies of the DFIG-based Wind Energy Conversion System (WECS) is shown in Fig. 6 (Alyousuf & Korkmaz, 2023; Dai & Tung, 2017; Le et al., 2016). The control system is divided into two parts: the first part is the electrical control system of the DFIG, which involves controlling both the RSC and GSC. The RSC's objective is to enable decoupled control of active and reactive power or speed for the DFIG wind turbine, while the GSC's objective is to maintain the DC-link voltage at a specified value, regardless of the magnitude and direction of the rotor power. The second part is the mechanical control system of the wind turbine, with the primary goal of maximizing wind power capture and minimizing transient low-speed shaft loads. All wind turbines have a terminal voltage of 0.69 kV, 12 poles, and a power factor of 0.95. The output voltage is stepped up to 22 kV and further stepped up to 220 kV via a step-up transformer to connect to the 220 kV transmission line.

Wind speed is a stochastic variable used to forecast the generating capacity of wind farms. The output power of a wind turbine is determined by the following equations (Kou et al., 2020; Nishikata & Tatsuta, 2025)

$$P_{WT} = \begin{cases} 0, & v_w < v_{cut-in} \\ P_{rated} \cdot \frac{v_w - v_{cut-in}}{v_{rated} - v_{cut-in}}, & v_{cut-in} \le v_w < v_{rated} \\ P_{rated}, & v_{rated} \le v_w \le v_{cut-out} \\ 0, & v_w > v_{cut-out}, \end{cases} \quad (4)$$

where v_w - the wind speed; P_{WT} is the output power of a wind turbine; P_{rated} - the rated power of the turbine; v_{cut-in}, v_{rated}, and $v_{cut-out}$ - the cut-in, rated, and cut-out wind speeds, respectively; P_{WT} - the output power of a wind turbine.

The output power of a wind farm can be calculated as

$$P_{WF} = \sum_{i=1}^{n} P_{WT,i}, \quad (5)$$

where n - the number of turbines in the wind farm.

Fig. 7 illustrates the forecasted 24-hour wind speed profiles for several major wind farms in the study area, with speeds ranging from 5.6 m/s to 13 m/s. This figure focuses on the wind speed at Buon Kuop WF. It shows how the wind speed changes throughout the day. In the morning, the wind speed is low due to cooler temperatures. As the sun rises and the land heats up, the

wind speed increases, peaking around 5 PM when the temperature reaches its highest point. Afterward, the wind speed gradually decreases in the evening as the temperature drops and the atmosphere stabilizes.

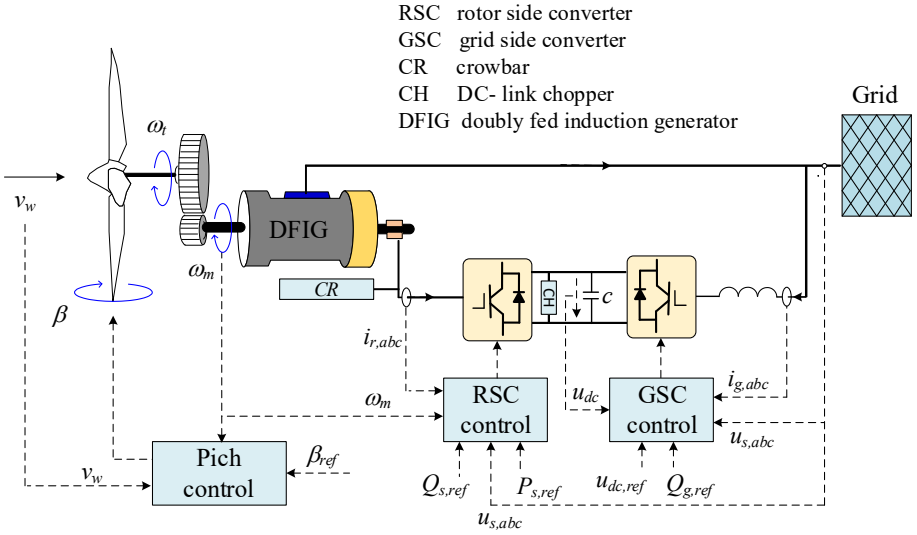

Fig. 6. The control system and grid connection of a wind power turbine

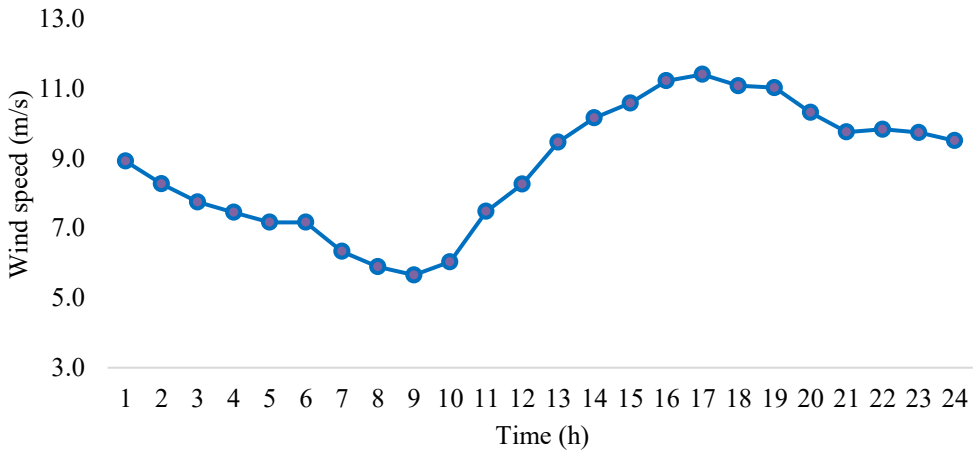

Fig. 7. The 24-hour speed of wind across the Buon Kuop wind farm

3. METHODOLOGICAL FRAMEWORK

With the geographical location of power source projects connected along the North-South transmission axis, when renewable energy plants come into operation, they will create transmission congestion points in the electrical system. The Tay Nguyen is an area that concentrates a large amount of capacity from wind and solar energy (Thanh et al., 2025). This will lead to internal grid congestion in the Tay Nguyen and also along the North-Central-South transmission sections, which is unavoidable. To prevent this issue from occurring in the system, multiple measures are needed. However, calculating the curtailment of renewable energy output to the grid is an urgent necessity.

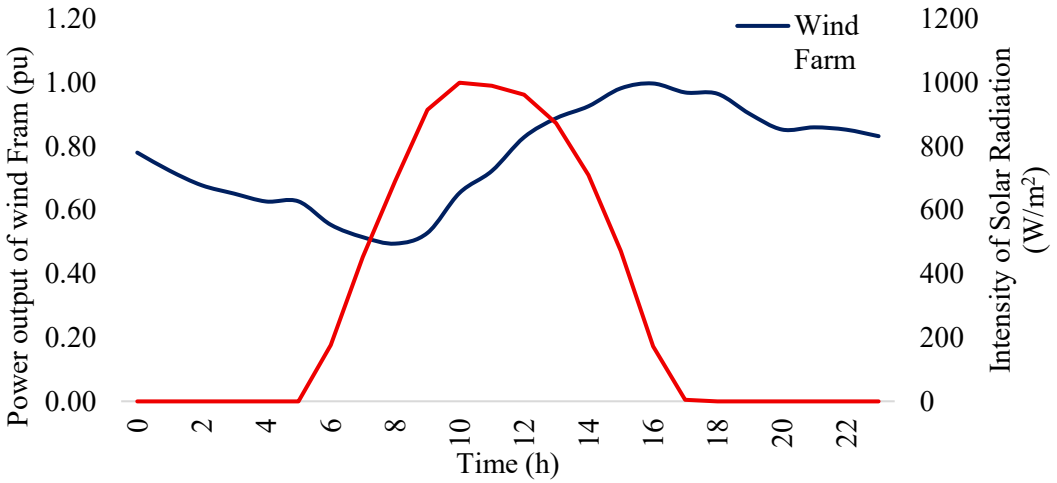

Fig. 8. The typical 24-hour power generation profiles of RESs

The calculation of renewable energy curtailment in a system with wind and solar energy sources needs to be considered from the perspective of overall coordination of the different operational patterns between wind power plants and solar power plants, which vary daily. This study presents typical results from regions significantly impacted by renewable energy sources. The output capacity of renewable energy sources, as shown in Fig. 8, is considered for calculation. In addition, the load of the three Tay Nguyen provinces, which has characteristics changing inversely with the generation capacity of renewable energy sources, as shown in Fig. 9, is also taken into consideration. Fig. 10 presents the calculation results for the 220 kV grid linking the 500 kV Pleiku 2 substation to the 500 kV Dak Nong substation on a typical day at 11 AM on April 20, 2025, in a scenario without curtailment of capacity and without the installation of BESS equipment.

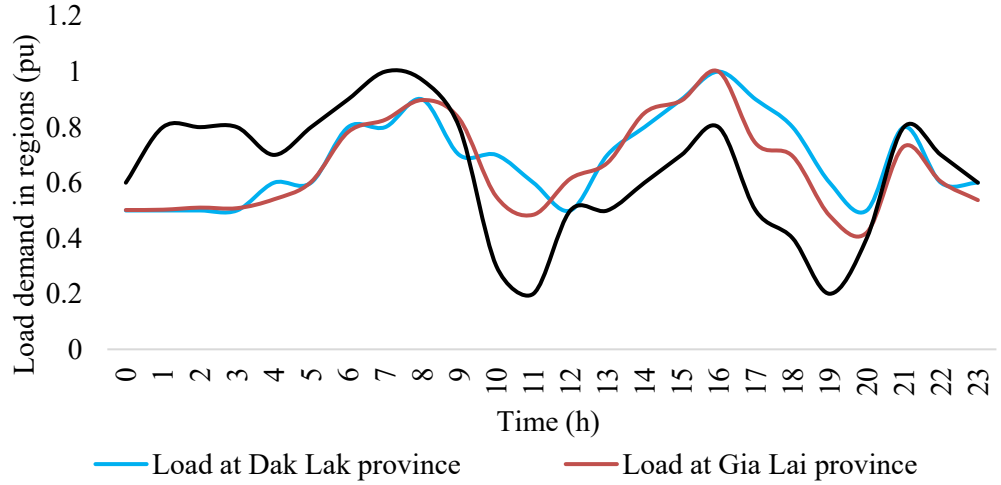

Fig. 9. The typical 24-hour load demand profiles of three provinces in the Tay Nguyen region, namely Dak Lak, Gia Lai, and Dak Nong

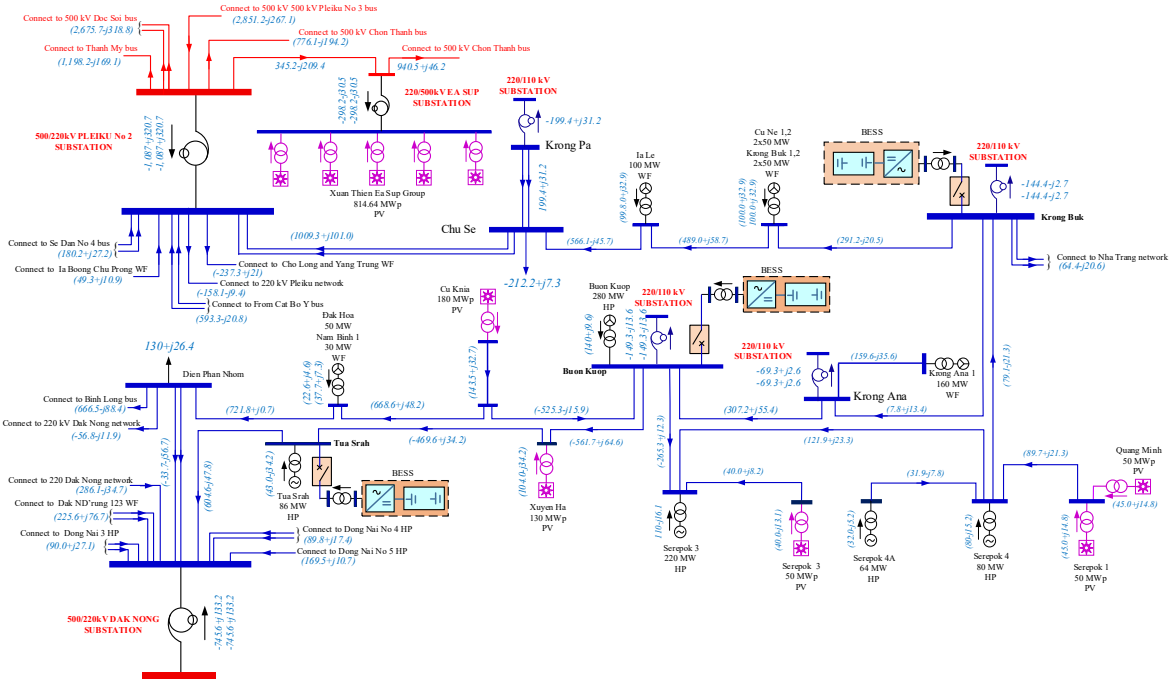

Fig. 10. The power distribution of the studied transmission network for a typical day at 11 AM on April 20, 2025

Fig.11 shows the power flow profiles at the Krong Buk and Pleiku 2 substations over a 24-hour period. At 9:04 AM, the power flow at Krong Buk begins to exceed the power flow limit (indicated by the dashed line), suggesting that the power generation from RES at this substation is approaching its maximum capacity. The power flow continues to rise and peaks at 12:01 PM, with an overload of 132.42%, reflecting a significant increase in power generation during this period. After the overload peak, at 1:51 PM, the power flow at Krong Buk decreases and returns below the power flow limit, indicating that the power generation in the area started to stabilize. The graph shows a decline in power flow, which could be due to reduced power generation. In contrast, Pleiku 2 maintains a stable power flow throughout the day, staying within the power flow limit, indicating that the power generation in this area is more stable and balanced.

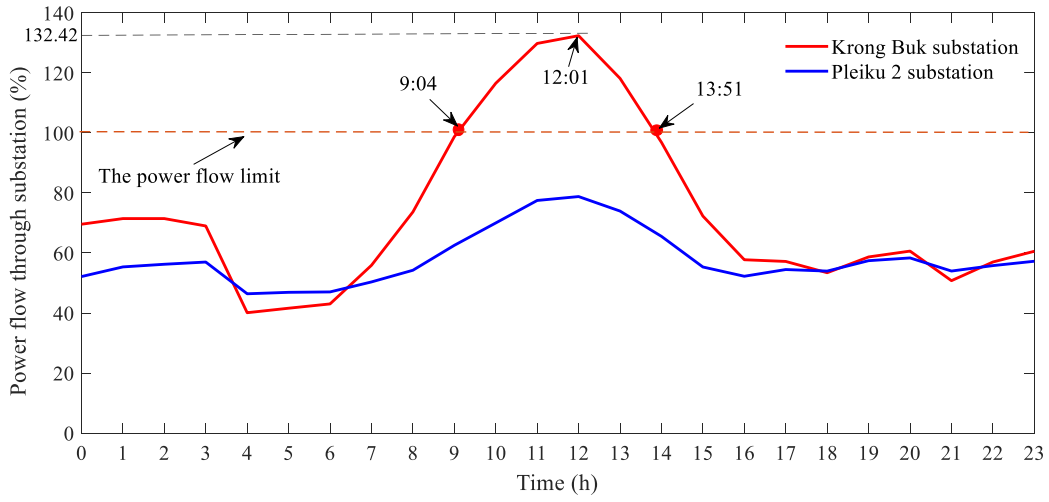

Fig. 11. The typical 24-hour power flow profiles through substations with no BESS

Fig. 12 presents the typical 24-hour power flow profiles on the 220 kV transmission lines of the studied transmission network. The results indicate that the connection line between the Pleiku 2 and Krong Buk substations becomes overloaded when RESs generate peak power, particularly on the Pleiku - Chu Se and Chu Se - Ia Le 220 kV transmission lines, with the overload reaching 125.8 % at 11:00 AM. Specifically, the power flow exceeds the limit at certain times, indicating that the power generation from RES is approaching its maximum capacity. This figure also shows that the Dak Hoa - Dien Phan Nhom and Turah - Dak Nong 220 kV transmission is experiencing overload. This indicates issues with the transmission capacity in this area. Other transmission lines, such as Buon Kuop - Xuyen Ha, maintain more stable power flows and do not exceed the power flow limit throughout the 24-hour period.

Fig. 13 illustrates the variation in power generation from RES over a 24-hour period. The results show that between 9:00 AM and 14:00 PM, power generation from RES, around 10,723 MWh, exceeds the grid's capacity to manage it, resulting in an excess power situation of approximately 2,057 MWh, as shown in the red diagonal area. This excess power needs to be reduced to prevent grid instability or overload. The light gray background represents the stable power range of about 8,667 MWh, which the grid can handle without any risk of overloading or system disruption, ensuring optimal performance of the grid.

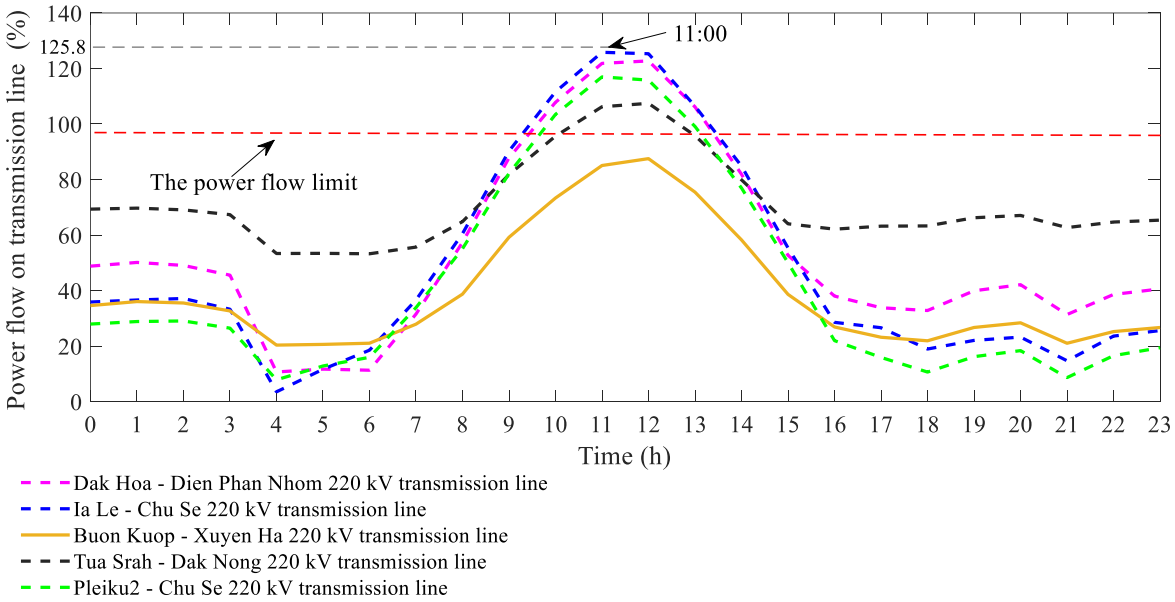

Fig. 12. The typical 24-hour power flow profiles on the 220 kV transmission line

4. THE PROPOSED METHOD

4.1. The BESS model

The BESS typically consists of three main components, as shown in Fig. 14. Firstly, the battery array, which includes multiple batteries connected in series to form rows and parallel connections between rows to form a cluster. Secondly, the power converter, which is a power

electronic converter that inverts DC current to AC for loads or the grid, or inverts AC current to DC for charging the battery array, operating based on control signals from the control and monitoring system. Thirdly, the control and monitoring system, which is the core of the BESS for regulating voltage, frequency, and power changes.

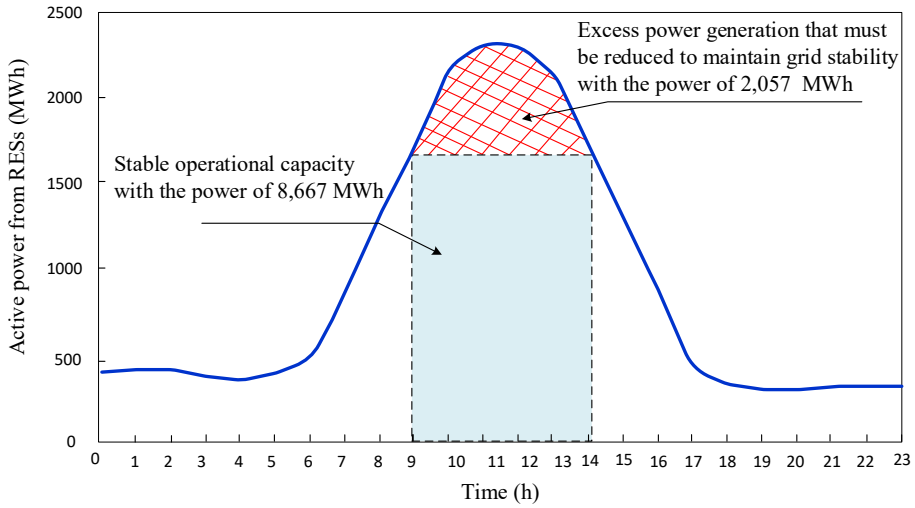

Fig. 13 The typical 24-hour power generation profiles of RESs

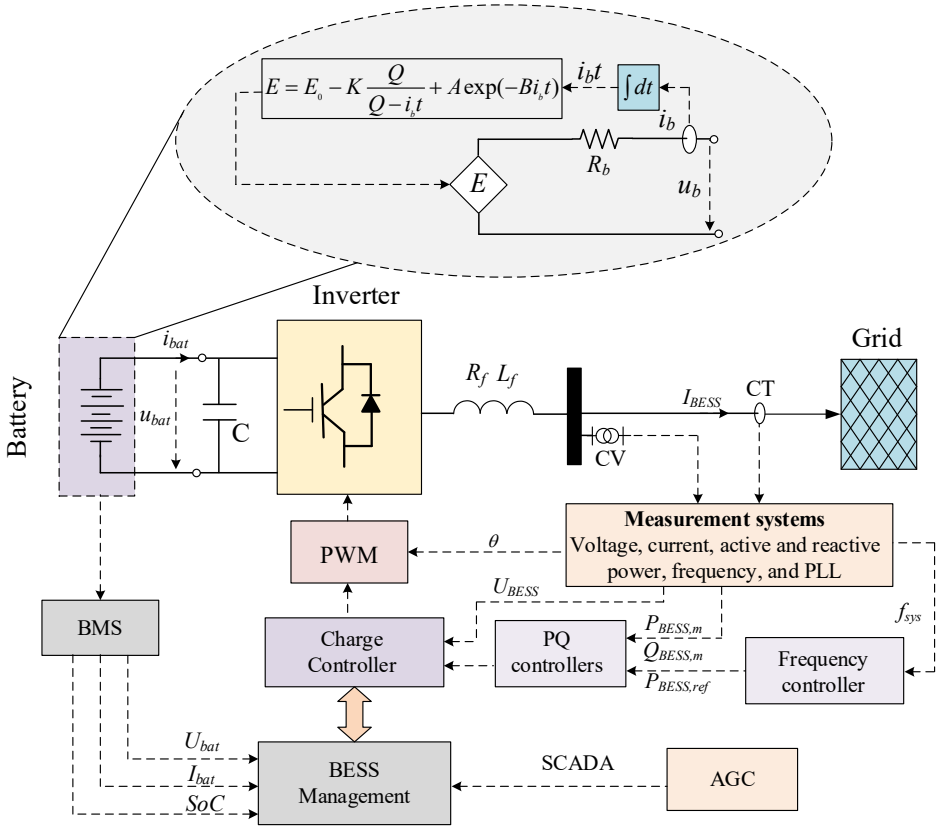

Fig. 14. The battery energy storage system (BESS) connected to the power grid

1) *The battery model*, which is a mathematical representation of a battery's behavior and characteristics, as can be seen in Zoom-out and can be described through the no-load voltage output as follows

$$E = E_0 - K \cdot \frac{1}{SoC} + A \cdot e^{-B \cdot Q \cdot (1 - SoC)}, \quad (6)$$

in which $(E_0 - K \cdot 1/SoC)$ - a voltage drop as battery's state of charge decreases; $\left(A \cdot e^{-B \cdot Q \cdot (1 - SoC)}\right)$ - an exponential behavior of the voltage with respect to the state of charge; E_0 - the baseline or reference voltage of the battery when the state of charge is fully charged; K - a constant that influences the voltage drop as the SoC decreases; SoC - the state of charge of the battery, representing the remaining charge in the battery as a percentage (ranging from 0 to 1, where 1 means fully charged); Q - a parameter that influences the exponential term, representing the battery's total charge capacity or another related factor, A - a constant that affects the second term of the equation, linked to the exponential behavior of the battery voltage; B - a constant affecting the exponential decay of the battery's voltage as SoC decreases. SoC is calculated as follows (Saha & Haque, 2021)

$$SoC(t) = SoC(t-1) + \frac{\eta_{charge} P_{charge}(t) - \frac{P_{discharge}(t)}{\eta_{discharge}}}{C_{rated}} \Delta t, \quad (7)$$

where η_{charge} and $\eta_{discharge}$ - the efficiencies of the charge and discharge processes, respectively; $P_{charge}(t)$ and $P_{discharge}(t)$ - the charge and discharge powers at time t, respectively; C_{rated} - the rated energy capacity; Δt - the time step.

2) *BESS control*, that is very important for making power grids with a lot of renewable energy more stable and efficient when it comes to transmission. BESS helps keep the grid stable during abrupt power outages by providing inertial response and frequency response. This helps reduce frequency fluctuations. The BESS control approach includes finding out how much power and capacity are required, utilizing Prony analysis to locate the optimal spot to deploy the system, and altering the charging and discharging according to how much demand there is for grid and renewable energy. This lets us use as much renewable energy as possible without overwhelming the grid. Fig. 14 shows that the BESS control system is made up of five independent parts. The following is a thorough list of the content:

a) Frequency control, which is applied to generate reference active power injected into the grid, utilizes a control loop based on frequency input signals, as shown in Fig. 15. The active power injected into the network by BESS is determined as follows (Silva Jr & Assis, 2020)

$$P_{bess,ref} = (p_{IR} + p_{PFR}) \cdot S_{BESS}, \quad (8)$$

where S_{BESS} - the rated power of BESS; p_{IR} and p_{PFR} - the active power signals obtained from the Inertia response (IR) and the primary frequency response (PFR) loops, respectively. The IR component provides rapid power injection/absorption proportional to RoCoF, while the PFR

component provides sustained power proportional to the frequency deviation, ensuring comprehensive frequency support. These control signals are given by (Knap et al., 2016)

$$\begin{cases} p_{IR} = K_{IR} \cdot \frac{1}{1+s\tau_1} \cdot \frac{1}{1+s\tau_2} \cdot \frac{d(f_{sys})}{dt}, \\ p_{PFR} = \frac{(f_{sys}-f_{ref})}{f_{ref} \cdot R_{BESS}}, \end{cases} \quad (9)$$

where K_{IR} - a gain of the inertial response control and R_{BESS} - the synthetic BESS droop.

The controller design for the BESS is based on a grid voltage imbalance event, as illustrated in Fig. 15 (Akram et al., 2020). The frequency response in the grid following a fault consists of several key stages. The first stage is the IR, which is the natural reaction of synchronous generators within the first 10 s to mitigate the initial frequency drop. Next, the PFR adjusts the frequency back to an acceptable level within 30 s using primary energy reserves. The magnitude and duration of IR and PFR deployment determine the frequency nadir, the lowest point of the frequency during recovery. The subsequent stage, secondary frequency response (SFR), further enhances frequency stability over a period of several minutes to 15 minutes. Finally, the tertiary frequency response (TFR) adjusts the output of energy sources over a longer period to fully restore grid stability. Each stage plays a crucial role in maintaining stability and preventing the risk of system collapse

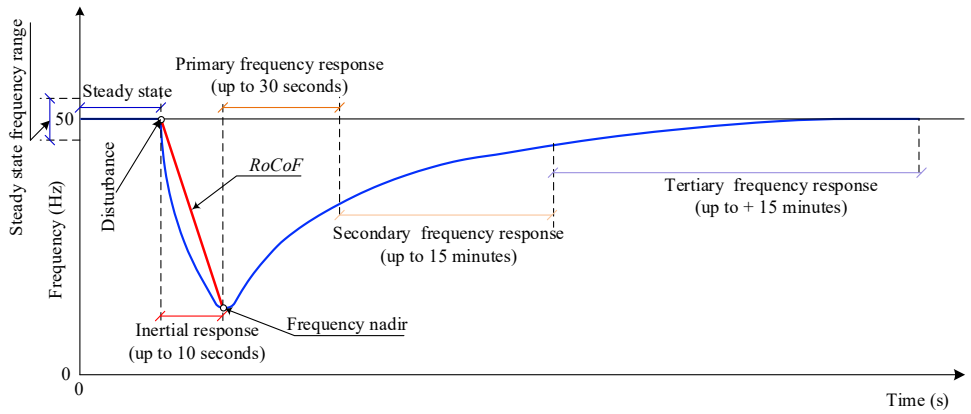

Fig. 15. Frequency response based on the European Network of Transmission System Operators for Electricity

b) Active and reactive power controllers, which denoted as *P* and *Q* controllers, are implemented to generate the *dq*-axis reference current components using proportional-integral (PI) control, as illustrated in Figs. 16 (b) and (c), respectively. The reference power output signal from the frequency controller, shown in Fig. 16 (a), is fed into the input of the active power controller. This signal is compared with the measured BESS power output to generate an active power error. This error signal passes through a low-pass filter and is combined with the Δi_d signal from the output of the charge controller in Fig. 16 (d). The combined signal is then added as a feedback signal to the PI controller, and the output signal is the d-axis reference

current, which serves as the input signal to the charge controller. Conversely, the voltage error signal between the reference and measured signals at the BESS connection point is processed in a similar manner. The error signal is passed through a low-pass filter and combined with the Δi_q signal from the output of the charge controller in Fig. 16 (d). This combined signal is fed back to the PI controller, and the output signal is the q-axis reference current, which is provided as an input to the charge controller.

c) Charge or discharge controller, the charge or discharge logic ensures the BESS operates within its *SoC* limits while meeting grid needs. Charging typically occurs during periods of excess RES generation or low demand, while discharging supports the grid during generation deficits or high demand (Yang et al., 2023). These actions can be governed by grid conditions, such as transmission line loading (Yang et al., 2023).

The charging condition of the BESS occurs when the power from the RES exceeds the total system power required, including the load and any losses. This indicates that there is surplus energy from RES that can be stored in the battery. The charging condition is defined as follows:

$$P_{BESS}(t) = min\left(P_{max\_charge}, P_{RES}(t) - P_{load}(t) - P_{loss}(t)\right), \quad (10)$$

and charging only occurs when meeting the following condition

$$P_{RES}(t) > P_{load}(t) - P_{loss}(t), \quad (11)$$

where $P_{RES}(t)$ - the power from renewable energy sources; $P_{load}(t)$ - the power required by the load; $P_{loss}(t)$ - the power loss in the system; P_{max_charge} - the maximum charging power of the BESS; when the condition in Eq. 11 is satisfied, the system will charge the BESS with the excess power.

The discharging condition of the BESS happens when the power from RES is insufficient to meet the load and losses. In this case, the system will discharge the battery to supply the grid. The discharging condition is given by

$$P_{BESS}(t) = -min\left(P_{max\_discharge}, P_{load}(t) + P_{loss}(t) - P_{RES}(t)\right), \quad (12)$$

and discharging occurs when the following condition is satisfied:

$$P_{RES}(t) < P_{load}(t) + P_{loss}(t), \quad (13)$$

where $P_{max\_discharge}$ - the maximum discharging power of the BESS; when condition in Eq. 13 is met, the BESS will discharge energy to supply the load.

From the left side of Fig. 16 (d), the SoC of the BESS is critical in ensuring that the system operates safely. The SoC must stay within the allowable limits, typically defined ($SoC_{min} < SoC < SoC_{max}$). If the *SoC* exceeds the maximum or drops below the minimum, the

system will stop charging or discharging to prevent damage to the battery.

d) Current control on the dq-axis, the right side of Fig. 16 (d) shows the *dq*-axis current in the BESS system. The current controller on *dq*-axis was applied to manage the current on the dq-axis, using the signals $i_{d,ref}$ *and* $i_{q,ref}$. It ensures that the current in the system stays aligned with the reference values, which are calculated based on conditions like the battery's SoC. The PI controllers were applied to maintain the system's current at values that match the reference currents and generate control signals m_d and m_q, which are then modulated via PWM to control the power components in the system.

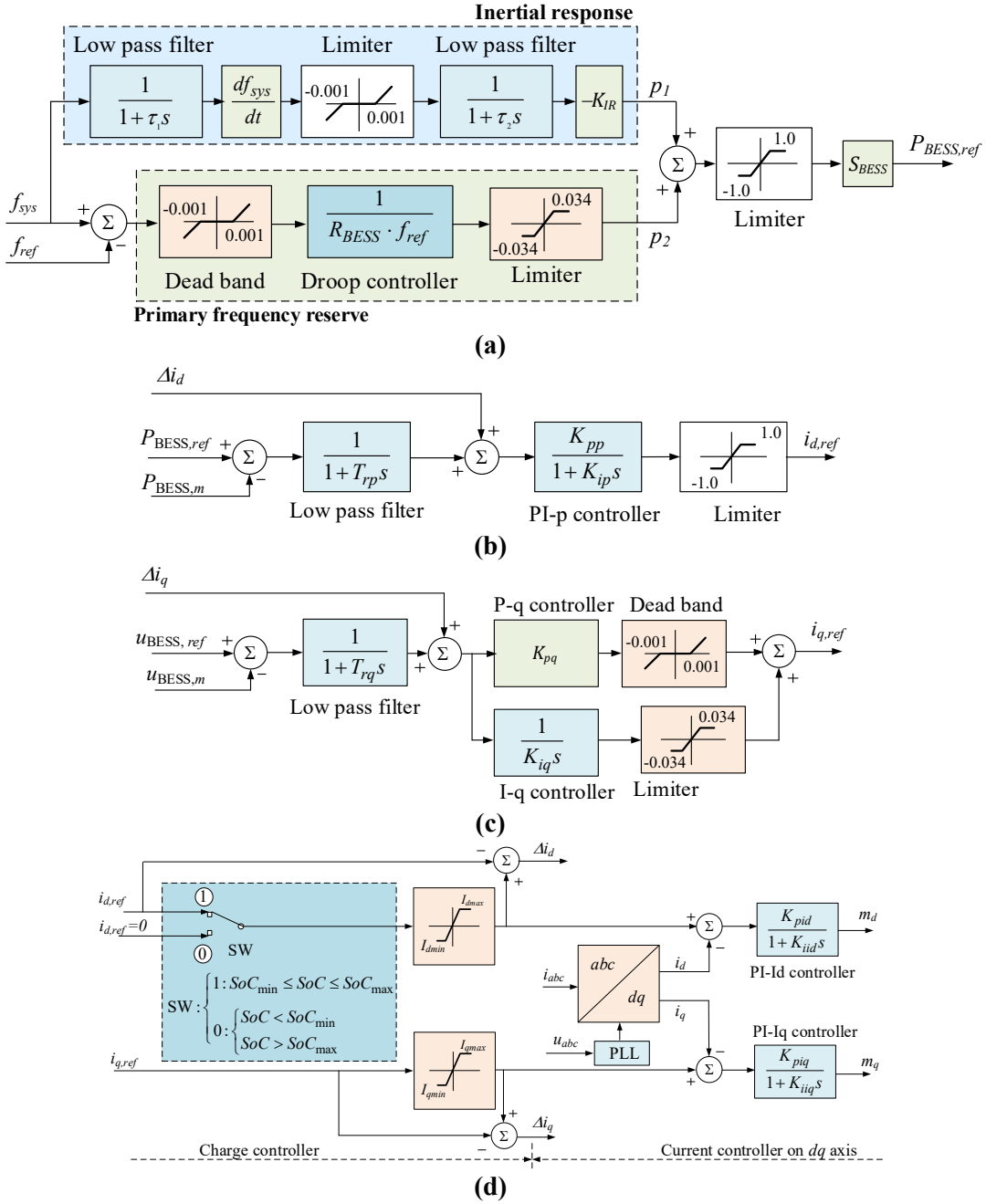

Fig. 16. BESS control: (a) Frequency control; (b) Active power controller; (c) Reactive power controller; (c) Charge or discharge controller and current controller of dq-axis

4.2. BESS Sizing

The size of BESS has to be calculated, including its power and energy capacity to alleviate grid frequency concerns. In grids with large amounts of RES, we determine the required capacity to limit the RoCoF and steady-state frequency variation. This ensures the BESS can rapidly inject or absorb power to stabilize the grid during sudden disruptions, such as the loss of a generator. To guarantee frequency stability, sizing involves determining the BESS's power rating and energy capacity (Liu et al., 2023; Rietveld et al., 2020). This process begins with understanding the dynamics of grid frequency, which are governed as follows: :

$$\frac{2H_{\text{sys}}}{f_0} \cdot \frac{df}{dt} = \frac{P_g - P_l}{S_{\text{sys}}} = \frac{\Delta P}{S_{\text{sys}}}, \quad (14)$$

where H_{sys} - system inertia constant; f_0 - nominal frequency; (df/dt) - the rate of change of frequency; P_g and P_l - the generation and load powers, respectively, represents system capacity; ΔP - power imbalance. The system inertia constant H_{sys} - calculated as the weighted average of the inertia constants H_i of individual synchronous generators based on their rated capacities S_i and can be determined as follows (Peng et al., 2024):

$$H_{sys} = \frac{\sum_{i=1}^{n} H_i \cdot S_i}{S_{sys}}, \quad (15)$$

where S_i and H_i - the rated capacity and inertia constant of the i^{th} generator, respectively. High RES penetration reduces H_{sys}, making the system more vulnerable to large $RoCoF$ and frequency deviations (Liu et al., 2023). BESS counters this by providing synthetic IR and fast PFR.

a) Sizing for inertial response, to prevent unwanted relay operations and ensure stability, the $RoCoF$ must be limited, typically to within ±0.5 Hz/s (Knap et al., 2016). The minimum aggregated inertial contribution required from BESS (H_{BESS}, S_{BESS}) to meet the maximum allowable $RoCoF$ $(RoCoF_{max})$ following a maximum power contingency (ΔP_{max}) is (Knap et al., 2016):

$$\sum_{i=1}^{m} H_{BESS_i} S_{BESS_i} \geq \frac{\Delta P_{max} f_0}{2RoCoF_{max}} - \sum_{i=1}^{n} H_i S_i, \quad (16)$$

where m is the number of BESS units; H_{BESS_i} and S_{BESS_i} are the i^{th} BESS inertia constant and capacity, respectively; $\Delta P_{\text{max}} f_0$ - maximum contingency power; $(RoCoF_{max} = df_{max}/dt)$ - maximum allowable $RoCoF$. The IR power provided by a BESS is proportional to the measured $RoCoF$ and can be determined as Eq.9 (Knap et al., 2016):

b) Sizing for primary frequency response, BESS must also contribute to arresting the frequency drop and minimizing the steady-state frequency deviation (Δf_{SS}). The steady-state frequency deviation following a power imbalance ΔP depends on the aggregated droop response of all

participating generators and BESS (Assery et al., 2023; Yoo et al., 2020):

$$\Delta f_{SS} = \frac{\Delta P}{\sum_{i=1}^{n} \frac{S_{BESS_i}}{R_{BESS_i} f_0} + \sum_{j=1}^{m} \frac{1}{R_j} \frac{S_j}{f_0} +}, \quad (17)$$

where R_{BESS_i} and R_j - the droop constants of the i^{th} BESS and j^{th} generator, respectively. To ensure the frequency remains above the minimum allowable limit (f_{min}), the minimum PFR contribution required from the BESS fleet by the following condition (Yoo et al., 2020):

$$\sum_{j=1}^{m} \frac{1}{R_{BESS_j}} \frac{S_{BESS_j}}{f_0} \geq \frac{\Delta P_{max}}{|f_0 - f_{min}|} - \sum_{i=1}^{n} \frac{S_i}{R_i f_0}. \quad (18)$$

The PFR power delivered by a BESS is proportional to the frequency deviation from nominal and can be determined as Eq. 9 (Assery et al., 2023; Yoo et al., 2020):

c) Total power and energy capacity, the total instantaneous power required from the BESS is the sum of its IR and PFR contributions as introduced in Eq. 8. The energy capacity must be sufficient to sustain this power output for the duration required for slower-acting reserves to respond, typically 10 - 30 s for IR and PFR roles, or longer depending on the application, such as peak shaving. The following condition calculates this energy capacity (Assery et al., 2023).

$$E_{bess} \geq P_{max} t_{duration}, \quad (19)$$

where P_{max} - the maximum required power output considering both p_{IR} and p_{PFR} demands during the contingency and $t_{duration}$ - the required response duration.

4.3. BESS Placement

The proper placement of BESS is crucial to maximise its impact. This study employs the Prony approach to analyze grid oscillations and identify optimal locations where BESS deployment can efficiently mitigate frequency fluctuations. Typically, these locations are situated near areas with high RES integration or where frequency variations are most severe (Tee et al., 2022). The optimal placement of BESS can provide its effectiveness in damping frequency oscillations, particularly in high-res grids. The Prony approach is utilized for oscillation analysis, splitting the frequency response signal into damped sinusoids (Xia et al., 2017; Nguyen et al., 2020)

$$\widehat{y_n} = \sum_{i=1}^{p} M_i e^{j\theta_i} e^{(\alpha_i + j2\pi f_i) n T_s}, n = 0, 1, 2, \ldots, N-1. \quad (20)$$

The eigenvalues λ_i is defined as

$$\lambda_i = (\alpha_i + j2\pi f_i). \quad (21)$$

$\widehat{y_n}$ will be presented as

$$\widehat{y_n} = \sum_{i=1}^{p} H_i e^{\lambda_i n T_s}. \quad (22)$$

The damping ratio for each mode is calculated as

$$\zeta_i = -\frac{\alpha_i}{\sqrt{\alpha_i^2 + (2\pi f_i)^2}}, \quad (23)$$

where $\widehat{y_n}$ - estimated signal of data sequence; p - model order; H_i - the residue of the i^{th} output includes the original input; M_i and θ_i - magnitude and phase at mode i^{th}, respectively; α_i and f_i - the damping coefficient and frequency, respectively; T_s - the time interval of sampling; N - the sampling number.

The process involves simulating a relevant contingency such as generator trip in the power system model; recording the dynamic frequency response or other relevant signals like bus voltage angles at candidate buses across the network; applying the Prony algorithm to the recorded signals from each candidate bus to identify the dominant oscillation modes and their characteristics, particularly the damping ratios and mode amplitudes; Identifying the mode with the lowest damping ratios like the most vital, lightly damped modes; choosing the optimal buses for BESS placement where the amplitude of the most critical mode is largest. Placing BESS at these buses affords the largest control action to damp the oscillations, thereby strengthening overall grid stability (Khunkitti et al., 2022).

4.4. Optimization and Simulation Workflow

The BESS has three basic components, including a battery storage system, an inverter/converter, and a control system, in which the battery storage system comprises many parallel and serial modules. Below is a complete description of the process as illustrated in Fig.17, explaining each step extensively to guarantee the BESS is correctly sized and positioned to sustain the grid during disturbances (Makarava et al., 2019).

Stat

Step 1, modeling the low-inertia grid with high-RES penetration.

Step 2, establishing performance criteria: maximum permissible *RoCoF* and steady-state frequency deviation ($\boldsymbol{\Delta f}_{SS}$).

Step 3, determining the needed BESS power and energy capacity using the sizing technique Eqs 14-19.

Step 4, running dynamic simulations of contingencies and using Prony analysis Eqs 20-23 to determine suitable BESS positions for dampening key oscillations.

Step 5, deploying the BESS model with the selected size, location, and control approach

Step 6, modeling situations with the BESS included into the grid.

Step 7, verifying frequency stability and other operating characteristics (e.g., line loading).

Step 8, iterating on size or placement if stability conditions are not fulfilled.

End

A 24-hour quasi-dynamic simulation is undertaken to examine the BESS performance under various daily RES production and load profiles, capturing its efficacy in controlling grid restrictions including transmission line and transformer overloads (Tee et al., 2022; Thanh et al., 2023).

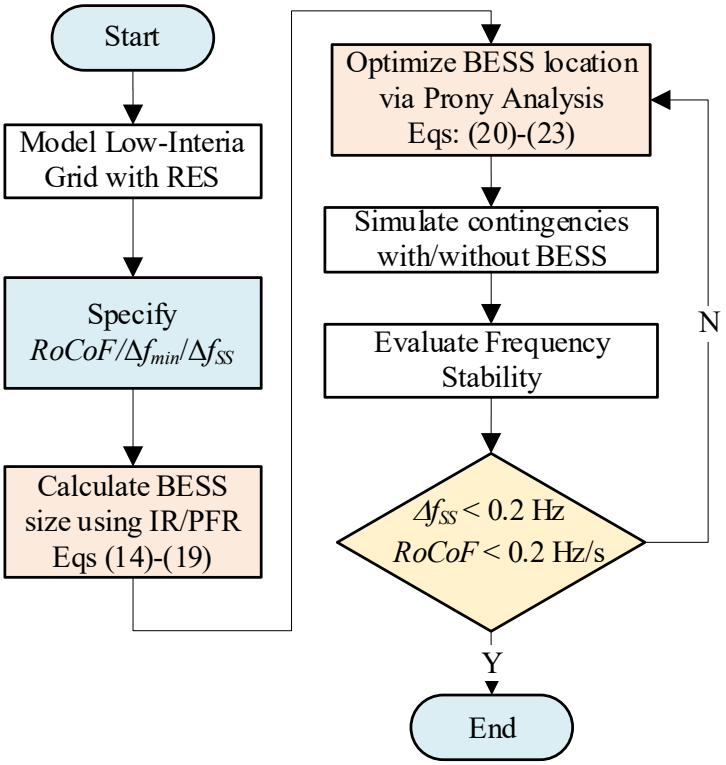

Fig. 17. Optimization workflow for BESS size and location

5. RESULTS

5.1. Simulation results for the power flow study with BESS

From the calculations in Section 3, it is evident that releasing capacity to the 500kV grid through the two stations, Pleiku 2 and Dak Nong, will cause the 220kV lines near these stations to become overloaded, such as the Dak Hoa - Luyen Nhom, Ia Le - Chu Se, Tua Srah - Dak Nong, and Pleiku 2 - Chu Se transmission lines. The calculation results show a corresponding daily output reduction of 2,057MWh, with the maximum required capacity reduction on this line axis being about 600MW, and the storage time is approximately 3.36-hour. By applying the method proposed in Section 4, it is calculated that three BESS units, each with a capacity of 200MW and 673MWh of energy storage, should be located at three positions: Krong Buk, Buon Kuop, and Tua Srah buses. The parameters related to the studied system are shown in Fig. 10, and the parameters of the BESS controller are listed in Table 1 and illustrated in Fig. 16.

Fig.18 shows the power flow fluctuations through the Krong Buk and Pleiku 2 substations after integrating three BESS substations. This result clearly demonstrates the effectiveness of the BESS, as the power flow through both substations always remains below the 100% threshold

for 24-hour. Continuous operation within the safety limit, together with a remarkably flat load curve, confirms that the BESS has successfully absorbed excess energy during off-peak hours and discharged it during peak hours. Technically, these results confirm that the BESS is a highly effective solution to optimize grid operations, solve local overload problems, and enhance both the reliability and safety of the power transmission system through improved energy management. Fig. 19 shows 24-hour power flow trends on the 220kV transmission lines after the integration of the BESS. The data reveals that power flows on all monitored lines stay constant and consistently below the 100% operating level throughout the day. This illustrates that the BESS effectively absorbs surplus energy during off-peak periods and supplies it during peak-demand, thereby relieving localized overloading. Scientific and technical perspective, BESS device can improve grid performance, safety transmission system, and permit more flexible energy management.

Table 1. The parameters of the BESS controller

Parameters	Value	Unit	Parameters	Value	Unit
The frequency controller			The charge/discharge controller		
τ_1	0.004	s	I_{dmin}	-0.4	pu
τ_1	0.0002	s	I_{qmin}	-1.0	pu
K_{IR}	2.5	-	I_{dmax}	1.0	pu
R_{BESS}	1.0	pu	I_{qmax}	1.0	pu
The active power controller			SOC_{min}	0	%
T_{rp}	0.01	s	SOC_{max}	100	%
K_{pp}	10	-	The current controller		
K_{ip}	2.5	-	K_{pid}	0.1	-
T_{rq}	0.1	s	K_{iid}	10	-
K_{pq}	10	-	K_{piq}	2.5	-
K_{iq}	75	-	K_{iiq}	200	-
The reactive power controllers					
T_{rq}	0.1	s			
K_{iid}	47	-			
K_{iq}	100	-			

5.2. Simulation results for the impact of cloud cover on the PV farm

This scenario analyzes the implications of rapid decreases in solar power generation due to cloud cover. As demonstrated in Fig. 20 (a), the sun irradiance significantly reduces from 1,000 W/m^2 at 2 s to 500 W/m^2 at 3 s. It continues to decline to 200 W/m^2 at 4 s, and approaches a full loss of coverage at 5 s. As the cloud cover disperses, the irradiance progressively rises to 800 W/m^2 at 30 s, and completely recovers to 1000 W/m^2 by 50 s. This scenario represents a negative event inspired by real-world events, resulting in a considerable fall in solar irradiance and, subsequently, a severe decrease in power generation from the six PV farms feeding the grid, as illustrated in Fig. 20 (b). At 5 s, the active power output decreases dramatically from

978 MW to 0.0 MW. After this, when the clouds dissipate, the clear sky permits maximum solar irradiance, resulting in a rise in power production and stability at 50 s. When power from the solar farms suddenly drops, the system frequency will decrease due to the power shortage. As shown in Fig. 21, in the absence of BESS, the frequency will fluctuate and drop below 48.91 Hz, causing instability. However, when BESS is present, the energy storage system will discharge electricity into the grid to compensate for the power shortage, helping to maintain a stable frequency with a minimum value of 49.17 Hz, ensuring stable conditions (BCT, 2016). and quickly recovering to 50 Hz**.**

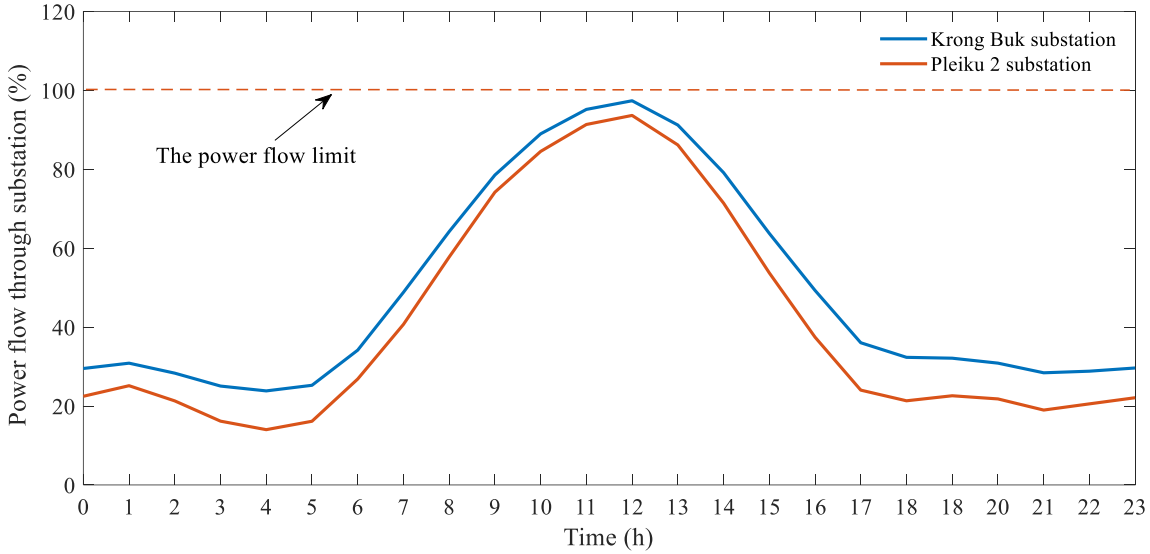

Fig. 18. The typical 24-hour power flow profiles through substations after connecting BESS

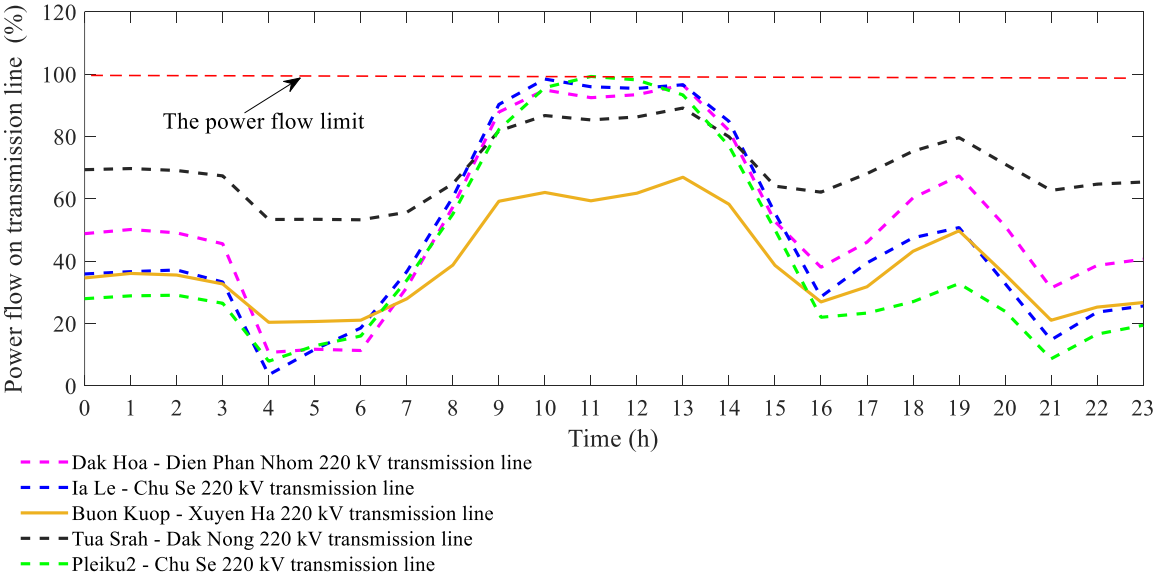

Fig. 19. The typical 24-hour power flow profiles on the 220 kV transmission line after connecting BESS

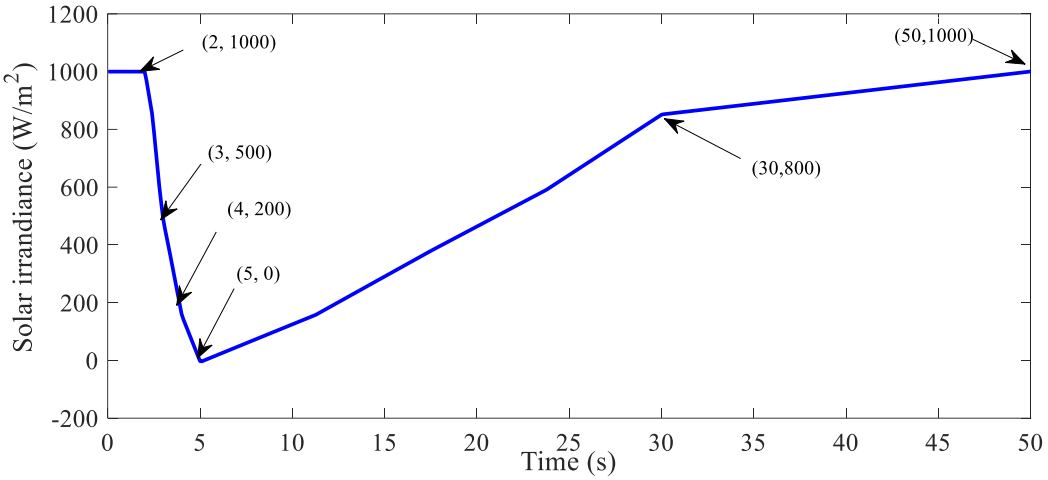

(a)

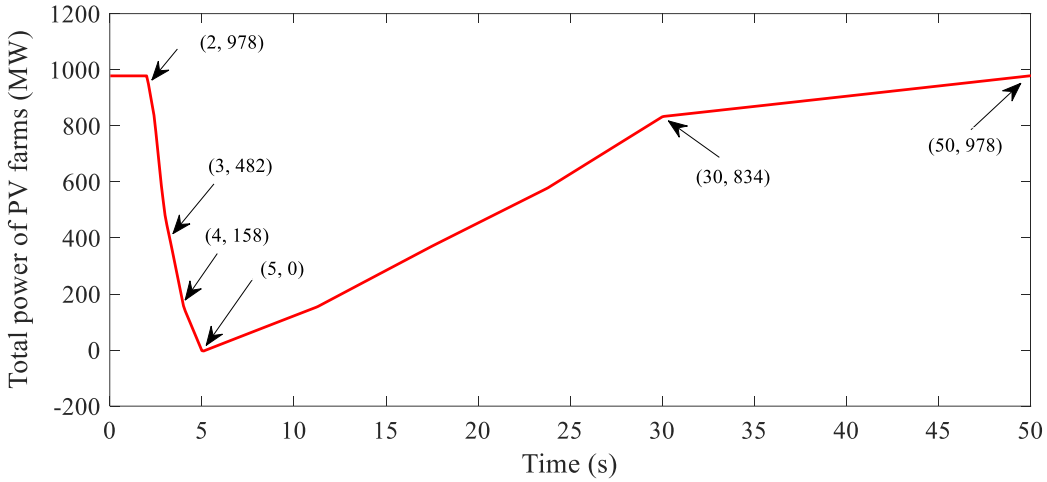

(b)

Fig. 20. The effect of cloud cover on solar farms: (a) radiation intensity; (b) total output power of PV farms

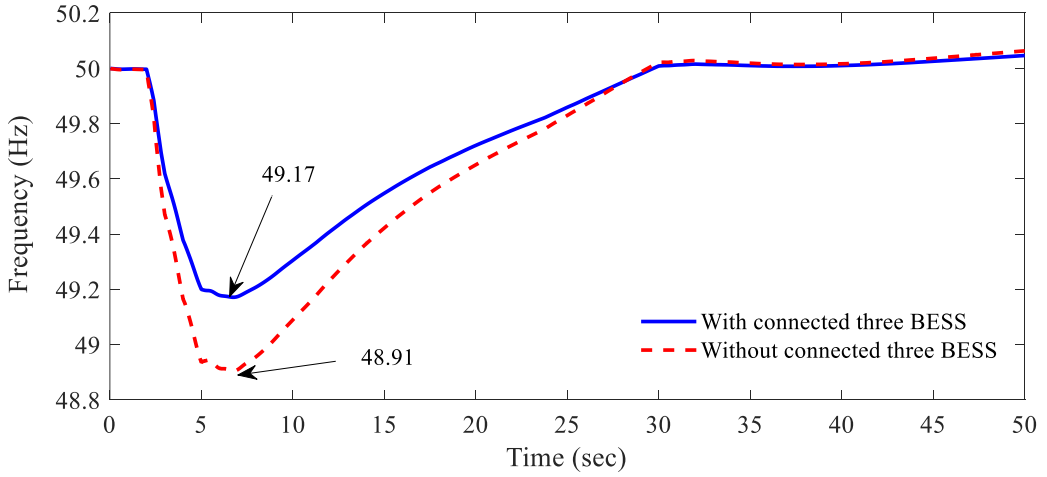

Fig. 21. The system frequency response

As shown in Fig. 22 (a), when the power from the PV farms decreases due to cloud cover, the BESSs start to discharge power to the grid to compensate for the power shortage. The discharge power peaks at around 5 s, with 178 MW from the BESS at Buon Kuop, 174 MW from the BESS at Krong Buk, and 169 MW from the BESS at Buon Tua Srah. All three BESS stations

provide similar amounts of discharge power, with Buon Kuop contributing the highest amount. After the PV power decreases and reaches 10 s, the discharge power from the BESSs starts to decrease as solar radiation begins to recover. Once the PV power is fully restored, the BESSs stop discharging and enter the recharge state to prepare for the next power shortage situation. In Fig. 22 (b), the *SoC* of the BESS systems reflects the discharging and recharging process. Initially, the state of charge is 90.5% for each BESS station. However, as the BESSs discharge power to the grid to maintain stability, the state of charge drops to 79.9% at 28 s for Buon Kuop, 80.3% for Krong Buk, and 80.1% for Buon Tua Srah. After the PV power recovered and the BESSs stopped discharging, the charge state began to recover, reaching 80.1% for Buon Kuop bus, 80.4% for Krong Buk bus, and 80.2% for Buon Tua Srah bus at 50 s. This change in the charge state shows the ability of the BESS at each station to supply and recharge energy while maintaining the stability of the power system.

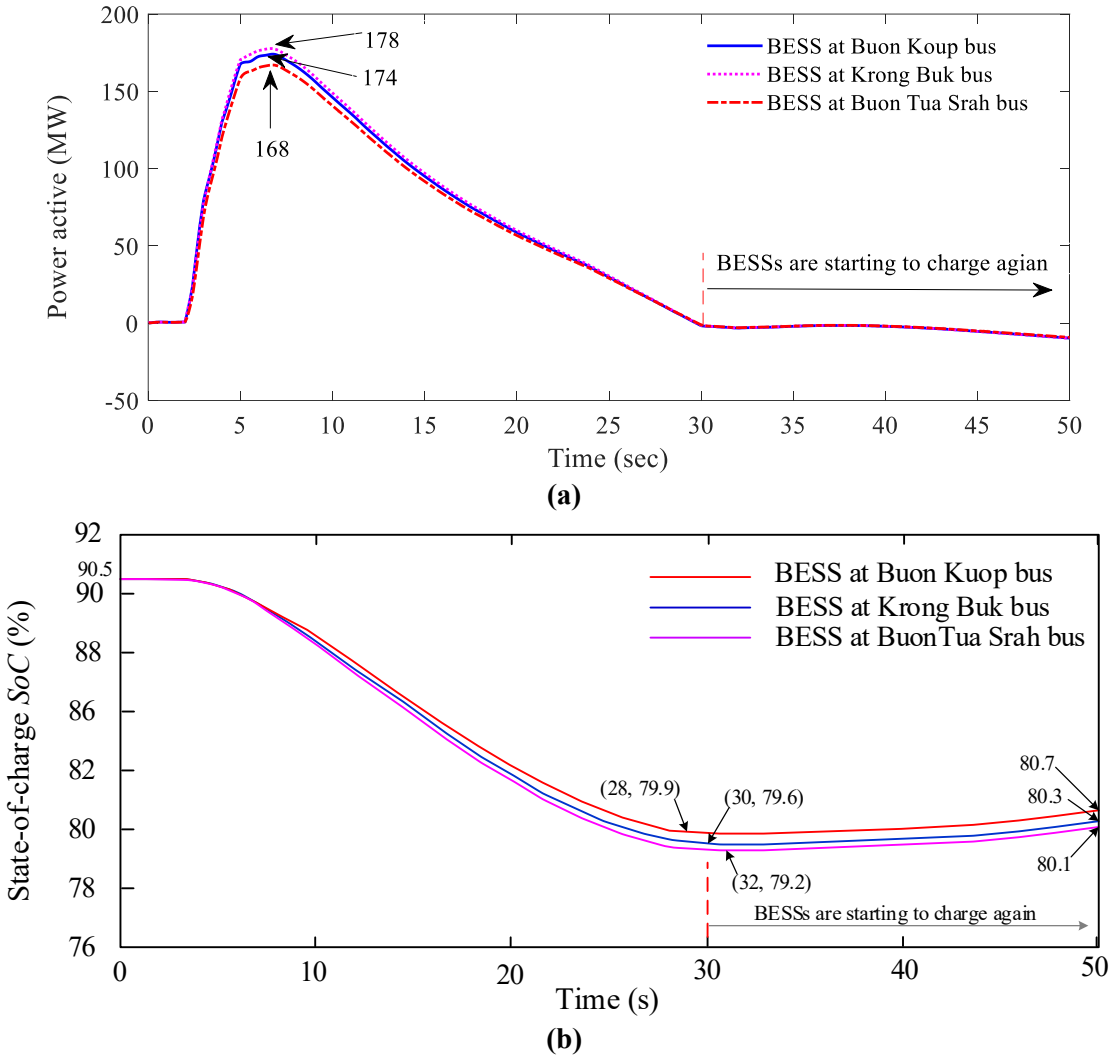

Fig. 22. Time-domain responses of BESS units: (a) active power; (b) state of charge

5.3. Simulation results during the grid fault

The system dynamics during a three-phase short circuit to earth on the Krong Buk - Serepok 4 line. This problem happens at 1 s near the Krong Buk bus. The fault lasts for 200 ms, and the line is then isolated to clear it. The voltage waveform at the short circuit location is illustrated in Fig. 23. Fig. 24 shows the active power provided by the BESS systems at various substations during a fault. At Krong Buk bus, the BESS provides -89.1 MW; at Buon Kuop, -105.4 MW; and at Tua Sam, -187.6 MW, indicating the amount of electricity discharged into the grid. These systems react promptly after the failure, with power outputs stabilizing within 1 - 2 s. The BESS maintains a stable power supply, providing voltage and frequency stability, and helps lessen the effect of the failure on the grid. This fast and persistent response highlights the BESS's efficacy in stabilizing the system and facilitating the introduction of renewable energy. For the case of a grid fault, as described in Fig. 23, the BESS immediately provides active power to support the system, as shown in Fig. 24, helping stabilize both voltage and frequency. Fig. 25 clearly displays the difference in frequency response with and without the BESS. In the case without the BESS, the frequency moves a lot about 53.98 Hz and takes longer to go back to normal. The BESS, on the other hand, keeps the frequency at 51.2 Hz and stabilizes it rapidly, at around 2 s. This reduces oscillations and keeps the grid stable. So, the BESS's ability to quickly provide power and stabilize frequency is very important for reducing the effects of grid fault situations.

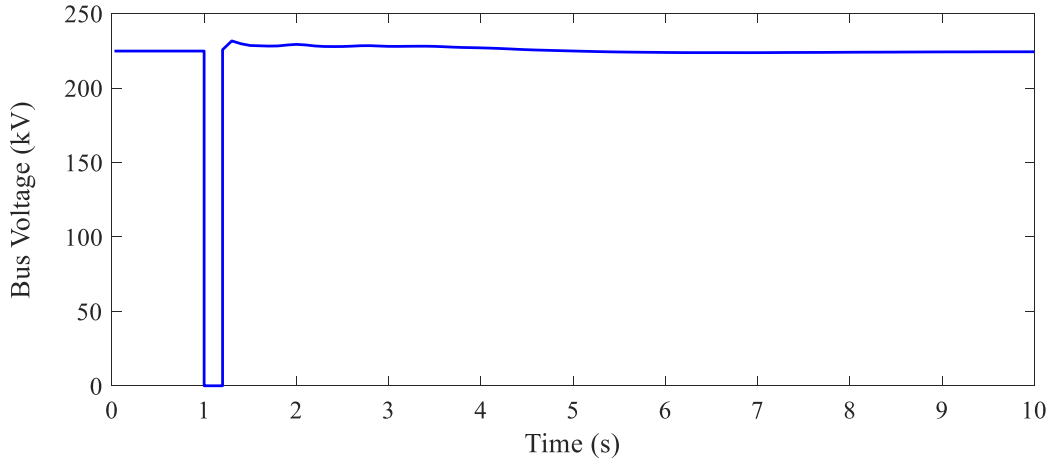

Fig. 23. Bus voltage response at the short-circuit point

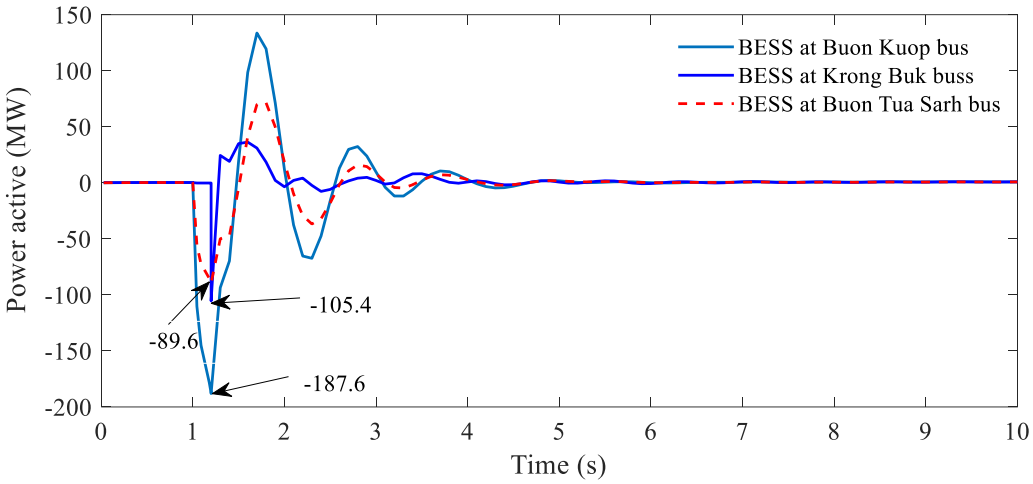

Fig. 24. BESS active power responses at selected buses

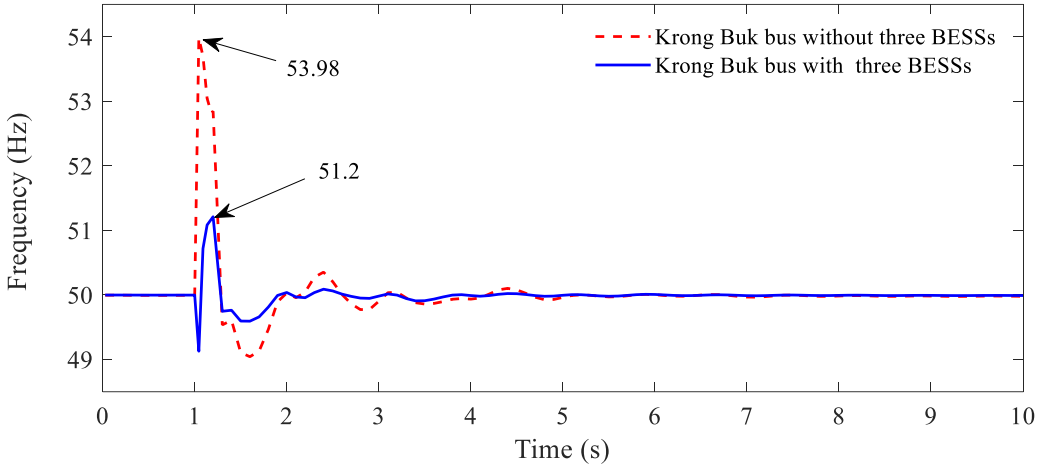

Fig. 25. Frequency response at the Krong Buk bus

6. CONCLUSIONS

Integrating utility-scale battery energy storage systems (BESS) into the 220 kV backbone is proposed here as a decisive fix for the stability issues hitting Vietnam's grid due to massive solar and wind integration. The paper focused our analysis on the Pleiku - Dak Nong corridor, a critical segment of the Tay Nguyen 220 kV network, where line overloads and frequency swings are most acute. The proposed control method connects virtual inertia with main frequency response, which is different from traditional setups. This allows the system to instantly absorb or inject power, smoothing out the unpredictable spikes from renewable sources.

To verify this, this paper ran heavy-duty simulations in both PSS/E and DIgSILENT PowerFactory. The data is clear; the BESS didn't just sit idle it handled a surplus of 2,057 MWh and kept the grid from crashing during faults. Specifically, it saw the frequency nadir improve from a dangerous 48.91 Hz to a much safer 49.17 Hz. These results prove the system can meet strict grid codes while tackling the intermittency problem. Future research steps involve stress-

testing this on the national scale and diving into grid-forming controls to see if the long-term investment holds up.

7. REFERENCES

Akram, U., Nadarajah, M., Shah, R., & Milano, F. (2020), "A review on rapid responsive energy storage technologies for frequency regulation in modern power systems", *Renewable and Sustainable Energy Reviews*, *120*, p.109626. https://doi.org/https://doi.org/10.1016/j.rser.2019.109626.

Al-Jabari, A., Korkmaz, F., & Teke, M. (2022), "A Simulation of solar energy system controlled by p&o, ic and fuzzy logic using bidirectional charging of battery", *Kufa Journal of Engineering*, *13*(3), pp.41-58. https://doi.org/https://doi.org/10.30572/2018/KJE/130303.

Alkahtani, M., Kamari, N., Zainuri, M., & Syam, F. (2024), "Design of grid-connected solar pv power plant in riyadh using PVsyst", *Energies*, *17*(24), p. 6229. https://doi.org/10.3390/en17246229.

Alsharif, H., Jalili, M., & Hasan, K. N. (2022), "Power system frequency stability using optimal sizing and placement of Battery Energy Storage System under uncertainty", *Journal of Energy Storage*, *50*, p.104610. https://doi.org/10.1016/j.est.2022.104610.

Alyousuf, A. M., & Korkmaz, F. (2023), "Performance investigation of wind turbines based on doubly fed induction generators with back-to-back converter", *Kufa Journal of Engineering*, *14*(1), pp.1-12. https://doi.org/10.30572/2018/KJE/140101.

Assery, S., Zhang, X.-P., & Chen, N. (2023), "Large-scale BESS for damping frequency oscillations of power systems with high wind power penetration", *Inventions*, *9*(1), p.3. https://doi.org/10.3390/inventions9010003.

BCT. (2016), "No. 25/2016/TT-BCT Regulations on Electricity Transmission System", *Ministry of Industry and Trade Circular*, Viet Nam. Retrieved November 30, from https://thuvienphapluat.vn/van-ban/Thuong-mai/Circular-25-2016-TT-BCT-regulations-electricity-transmission-system-339051.aspx.

Chen, S., Zhang, T., Gooi, H. B., Masiello, R. D., & Katzenstein, W. (2015), "Penetration rate and effectiveness studies of aggregated BESS for frequency regulation", *IEEE Transactions on Smart Grid*, 7(1), pp.167-177. https://doi.org/10.1109/TSG.2015.2426017.

Dai, L. V., & Tung, D. D. (2017). "Modeling for development of simulation tool: a case study of grid connected doubly fed induction generator based on wind energy conversion system". *International Journal of Applied Engineering Research*, *12*(11), pp.2981-2996.

Das, C. K., Mahmoud, T. S., Bass, O., Muyeen, S., Kothapalli, G., Baniasadi, A., & Mousavi, N. (2020), "Optimal sizing of a utility-scale energy storage system in transmission networks to improve frequency response", *Journal of Energy Storage*, 29, p.101315. https://doi.org/10.1016/j.est.2020.101315.

Dhaked, D., Dadhich, S., & Birla, D. (2023), "Power output forecasting of solar photovoltaic plant using LSTM", *Green Energy and Intelligent Transportation*, *2*(5), p.100113. https://doi.org/10.1016/j.geits.2023.100113.

El-Bidairi, K. S., Nguyen, H. D., Mahmoud, T. S., Jayasinghe, S., & Guerrero, J. M. (2020), "Optimal sizing of battery energy storage systems for dynamic frequency control in an islanded microgrid: A case study of flinders island, Australia", *Energy*, 195, p.117059. https://doi.org/10.1016/j.energy.2020.117059.

Frost, & Sullivan. (2024), "Growth opportunities for the grid-scale battery energy storage systems (BESS) industry", Researchandmarkets. https://www.researchandmarkets.com/reports/6008081.

Khunkitti, S., Boonluk, P., & Siritaratiwat, A. (2022), "Optimal location and sizing of BESS for performance improvement of distribution systems with high DG penetration", *International Transactions on Electrical Energy Systems*, *2022*(1), p.6361243. https://doi.org/10.1155/2022/6361243.

Knap, V., Chaudhary, S. K., Stroe, D. I., Swierczynski, M., Craciun, B. I., & Teodorescu, R. (2016), "Sizing of an energy storage system for grid inertial response and primary frequency reserve", *IEEE Transactions on Power Systems*, *31*(5), pp.3447-3456. https://doi.org/10.1109/TPWRS.2015.2503565.

Kou, P., Wang, C., Liang, D., Cheng, S., & Gao, L. (2020), "Deep learning approach for wind speed forecasts at turbine locations in a wind farm", *IET Renewable Power Generation*, *14* (13), pp.2416-2428. https://doi.org/10.1049/iet-rpg.2019.1333.

Le, V., Li, X., Li, Y., Dong, T. L. T., & Le, C. (2016), "An innovative control strategy to improve the fault ride-through capability of DFIGs based on wind energy conversion systems", *Energies*, *9*(2), p.69. https://doi.org/https://doi.org/10.3390/en9020069

Lee, J., Han, S., & Lee, D. (2023), "Optimizing the location of frequency regulation energy storage systems for improved frequency stability", *Batteries*, *9*(12), p.592. https://doi.org/10.3390/batteries9120592.

Li, S., Xu, Q., & Huang, J. (2023), "Research on the integrated application of battery energy storage systems in grid peak and frequency regulation", *Journal of Energy Storage*, *59*, p. 106459. https://doi.org/10.1016/j.est.2022.106459.

Liu, J., Wang, C., Zhao, J., & Bi, T. (2023), "RoCoF Constrained Unit Commitment Considering Spatial Difference in Frequency Dynamics, *Power Systems", IEEE Transactions on Power Systems*, *39*(1), pp. 1111-1125. https://doi.org/10.1109/TPWRS.2023.3240776

Maeyaert, L., Vandevelde, L., & Döring, T. (2020), "Battery storage for ancillary services in smart distribution grids", *Journal of Energy Storage*, *30*, p.101524. https://doi.org/10.1016/j.est.2020.101524.

Makarava, N., Lin, G., & Eichstädt, S. (2019), "Adaptive quasi-dynamic state estimation for MV and LV grids", *EURASIP Journal on Advances in Signal Processing*, *2019*, p.39. https://doi.org/10.1186/s13634-019-0628-2.

Xia, X., Li, X., & Ni, W. (2017), "Dominant low-frequency oscillation modes tracking and parameter optimisation of electrical power system using modified Prony method", IET Generation, Transmission & Distribution, *11*(17), pp.4358-4364. https://doi.org/10.1049/iet-gtd.2016.1436.

Nguyen, H. C., Tran, Q. T., & Besanger, Y. (2024), "Effectiveness of BESS in improving frequency stability of an island grid", *IEEE Transactions on Industry Applications*, *60*(6), pp.8203-8212. https://doi.org/10.1109/TIA.2024.3443241.

Nguyen, T. H., Yang, G., Jensen, P., Nielsen, A., & Pal, B. (2020), "Applying synchronous condenser for damping provision in converter-dominated power system," *Journal of Modern Power Systems and Clean Energy*, *9*(3), pp.639-647. https://doi.org/10.35833/MPCE.2020.000207

Nishikata, S., & Tatsuta, F. (2025), "Study on output power of wind farm composed of current-source series-connected wind turbines," *IEEE Transactions on Sustainable Energy*, *16*(3), pp.1827-1836. https://doi.org/10.1109/TSTE.2025.3537622.

Peng, L., Luo, L., Yang, J., & Li, W. (2024), "A wind power fluctuation smoothing control strategy for energy storage systems considering the state of charge," *Energies*, *17*(13), p.3132. https://doi.org/10.3390/en17133132.

Rietveld, G., Wright, P., & Roscoe, A. (2020), "Reliable rate of change of frequency measurements: use cases and test conditions," *IEEE Transactions on Instrumentation and Measurement*, *69*(9), pp.6657-6666. https://doi.org/10.1109/TIM.2020.2986069.

Sadeq Al Khdhairi, Y. M., & Vural, A. M. (2024), 'Nonlinear control of a two-stage 1-MWH grid-connected battery energy storage system by exact linearization via state feedback', *IETE Journal of Research*, *70*(1), pp.1015-1027. https://doi.org/10.1080/03772063.2022.2116360.

Saha, S., & Haque, M. M. (2021), "Post-Event restoration strategy for coupled distribution-transportation system utilizing spatiotemporal flexibility of mobile emergency generator and mobile energy storage system," *Electric Power Systems Research*, *199*, p.107432. https://doi.org/10.1016/j.epsr.2021.107432.

Silva Jr, S. S., & Assis, T. M. L. (2020), "Adaptive underfrequency load shedding in systems with renewable energy sources and storage capability", *Electric Power Systems Research*, *189*, p.106747. https://doi.org/doi.org/10.1016/j.epsr.2020.106747.

Tee, W. H., Ahmed Qaid, K., Gan, C., & Tan, P. H. (2022), "Battery energy storage system sizing using PSO algorithm in DIgSILENT PowerFactory", *International Journal of Renewable Energy Research*, 12(4), pp.2143-2151. https://doi.org/10.20508/ijrer.v12i4.13470.g8591.

Teh, J., & Lai, C.-M. (2019), "Reliability impacts of the dynamic thermal rating and battery energy storage systems on wind-integrated power networks", *Sustainable Energy, Grids and Networks*, *20*, p.100268. https://doi.org/10.1016/j.segan.2019.100268.

Thanh, T. V., Quyen, L. C., Viet, D. T., Hieu, N. H., & Dai, L. V. (2025), 'Advanced frequency control strategy for power systems with high renewable energy penetration: A battery energy storage system approach', *An International Journal of Optimization and Control: Theories & Applications, 15*(4), pp.625-648. https://doi.org/10.36922/ijocta025150076.

Thanh, T., Dinh, V., Quyen, L., Van Dai, L., & Tran-Quoc, T. (2023), "New method for secondary frequency regulation by battery energy storage system on Viet Nam power system" *2023 Asia Meeting on Environment and Electrical Engineering (EEE-AM)*, Hanoi, Vietnam, 2023, pp.1-6. https://doi.org/10.1109/EEE-AM58328.2023.10395758.

Tripathi, A., Aruna, M., & Suryanarayana Chivukula, M. (2018), "Output power enhancement of solar pv panel using solar tracking system," *Recent Advances in Electrical & Electronic Engineering*, 12(1), pp.45-49. https://doi.org/10.2174/2352096511666180501124714.

Vietnam-Prime-Minister. (2023), "Approving the national power development master plan for the 2021-2030 period, with a vision toward 2050, No. 500/QD-TTg", Retrieved May 15 from https://english.luatvietnam.vn/cong-nghiep/decision-500-qd-ttg-2023-national-power-development-master-plan-in-2021-2030-252621-d1.html.

Yang, J., Peng, L., Luo, L., & Yang, T. (2023), "Control strategy for energy-storage systems to smooth wind power fluctuation based on interval and fuzzy control", *IEEE Access*, *11*, pp.20979-20993. https://doi.org/10.1109/ACCESS.2023.3251113.

Yoo, Y., Jung, S., & Jang, G. (2020), "Dynamic inertia response support by energy storage system with renewable energy integration substation", *Journal of Modern Power Systems and Clean Energy*, *8*(2), pp.260-266. https://doi.org/10.35833/MPCE.2018.000760.